



Controllable Generation of Reactive Oxygen Species on Cyano-Group-Modified Carbon Nitride for Selective Epoxidation of Styrene

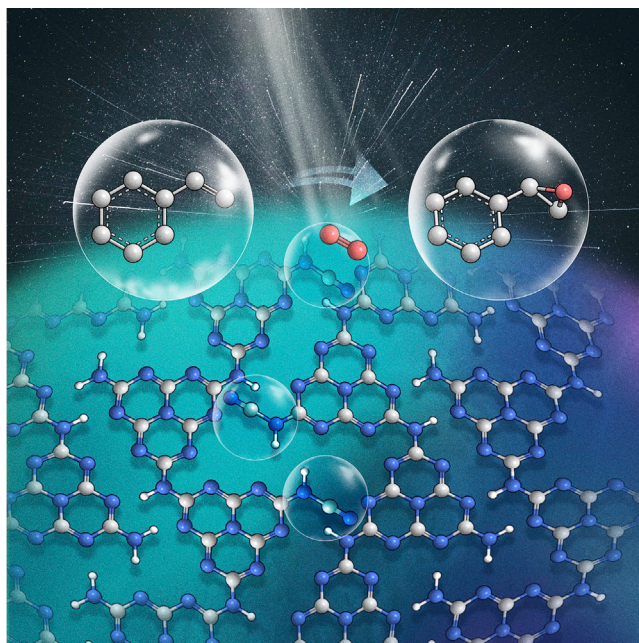
Hao Tan,^{1,3,5} Peng Kong,^{1,4,5} Riguang Zhang,⁴ Mengting Gao,^{1,3} Meixian Liu,^{1,3} Xianmo Gu,^{1,2,*} Weifeng Liu,² and Zhanfeng Zheng^{1,3,*}

*Correspondence: guxm@sxicc.ac.cn (X.G.); zfzheng@sxicc.ac.cn (Z.Z.)

Received: November 10, 2020; Accepted: January 30, 2021; Published Online: February 5, 2021; <https://doi.org/10.1016/j.xinn.2021.100089>

© 2021 The Author(s). This is an open access article under the CC BY-NC-ND license (<http://creativecommons.org/licenses/by-nc-nd/4.0/>).

GRAPHICAL ABSTRACT



PUBLIC SUMMARY

- Surface group modification is a significant strategy to improve catalyst activity
- Cyano groups are incorporated on the surface of carbon nitride via copolymerization
- Cyano group reactive sites allow high selectivity of styrene oxide for aerobic oxidation
- The system can be scaled up under solar light irradiation



Controllable Generation of Reactive Oxygen Species on Cyano-Group-Modified Carbon Nitride for Selective Epoxidation of Styrene

Hao Tan,^{1,3,5} Peng Kong,^{1,4,5} Riguang Zhang,⁴ Mengting Gao,^{1,3} Meixian Liu,^{1,3} Xianmo Gu,^{1,2,*} Weifeng Liu,² and Zhanfeng Zheng^{1,3,*}

¹State Key Laboratory of Coal Conversion, Institute of Coal Chemistry, Chinese Academy of Sciences, Taiyuan 030001, China

²Key Laboratory of Interface Science and Engineering in Advanced Materials, Ministry of Education, Taiyuan University of Technology, Taiyuan 030024, China

³Center of Materials Science and Optoelectronics Engineering, University of Chinese Academy of Sciences, Beijing 100049, China

⁴Key Laboratory of Coal Science and Technology of Ministry of Education and Shanxi Province, Institute of Coal Chemical Engineering, Taiyuan University of Technology, Taiyuan 030024, China

⁵These authors contributed equally

*Correspondence: guxm@sxicc.ac.cn (X.G.); zfzheng@sxicc.ac.cn (Z.Z.)

Received: November 10, 2020; Accepted: January 30, 2021; Published Online: February 5, 2021; <https://doi.org/10.1016/j.xinn.2021.100089>

© 2021 The Author(s). This is an open access article under the CC BY-NC-ND license (<http://creativecommons.org/licenses/by-nc-nd/4.0/>).

Citation: Tan H., Kong P., Zhang R., et al., (2021). Controllable Generation of Reactive Oxygen Species on Cyano-Group-Modified Carbon Nitride for Selective Epoxidation of Styrene. *The Innovation* 2(1), 100089.

The controlled generation of reactive oxygen species (ROS) to selectively epoxidize styrene is a grand challenge. Herein, cyano-group-modified carbon nitrides (CNCY_x and CN-T_y) are prepared, and the catalysts show better performance in regulating ROS and producing styrene oxide than the cyano-free sample. The *in situ* diffuse reflectance infrared and density functional theory calculation results reveal that the cyano group acts as the adsorption and activation site of oxygen. X-ray photoelectron spectroscopy and NMR spectrum results confirm that the cyano group bonds with the intact heptazine ring. This unique structure could inhibit H₂O₂ and ·OH formation, resulting in high selectivity of styrene oxide. Furthermore, high catalytic activity is still achieved when the system scales up to 2.7 L with 100 g styrene under solar light irradiation. The strategy of cyano group modification gives a new insight into regulating spatial configuration for tuning the utilization of oxygen-active species and shows potential applications in industry.

KEYWORDS: epoxidation; cyano modification; carbon nitride; ROS; steric hindrance

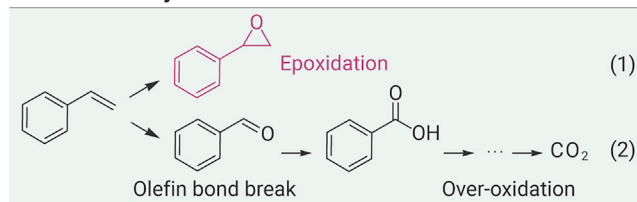
INTRODUCTION

Selective epoxidation of styrene by reactive oxygen species (ROS) originating from dioxygen is an economically important atomic reaction, and the styrene oxide products are versatile intermediates for the synthesis of perfumes, drugs, epoxy resins, and sweeteners and even for the chemical fixation of CO₂.^{1–3} The ROS mainly include superoxide anion radical (O₂^{·-}, Scheme 1, Equation 3),⁴ hydrogen peroxide (H₂O₂, Equation 4, or the intermediate peroxy species, -O-O-),⁵ hydroxyl radical (·OH, Equation 5),⁶ and singlet oxygen (¹O₂, Equations 8, 9, and 10, the energy transfer from the excited state of the sensitizer or O₂^{·-} oxidation product).^{7,8} Among all the ROS, -O-O- and ¹O₂ react with styrene via [2 + 2] photochemical cycloaddition and generate styrene oxide as the product.^{9,10} Yet, H₂O₂ and ·OH induce the olefin bond break and overoxidation reaction of styrene (Scheme 1, Equations 1 and 2),^{9,11} resulting in a low yield of styrene oxide (<50%) in most catalytic systems (16 catalytic systems are summarized in Table S1). Progress has been made on thermocatalysis and photocatalysis to achieve high epoxidation efficiency. For example, the transition-metal species, especially cobalt-based materials,^{12–14} WO₃/TiO₂ composite,¹⁵ CuNP/TiN₂ photocatalysts,¹⁶ VLB120 enzyme,¹⁷ etc., could drive the selective epoxidation of various alkenes with O₂ successfully. However, the toxicity of heavy metals and problem of enzyme recycling limit their application. Thus, it is desirable to design metal-free heterogeneous catalysts with high stability and recyclability. Moreover, a deep understanding of the ROS transformation mechanism is critical for catalyst engineering.

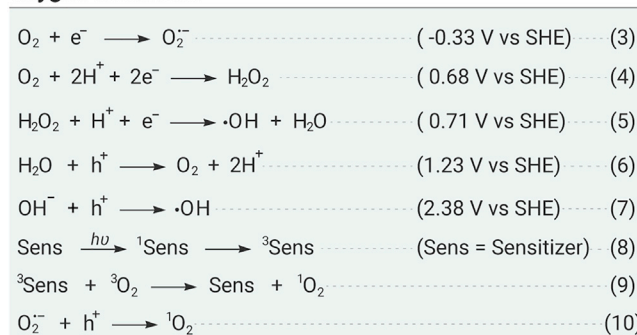
Polymeric carbon nitride has been widely investigated in the activation of molecular oxygen and in driving the corresponding aerobic oxidation reactions.^{4,5,7,18–22} It has been reported that the heptazine ring structure in carbon nitride can promote the two-electron reduction of oxygen and adjust H₂O₂ formation (Scheme 1, Equation 4).^{23,24} In addition, carbon nitride has exhibited high performance in ·OH generation (Equation 5) for photodegradation of organic contaminants.²⁵ However, these ROS are not favorable for the photocatalytic epoxidation of styrene reactions. A large amount of low-value benzaldehyde and benzoic acid are still formed, although various transition-metal cations (Fe³⁺, Mn²⁺, Co²⁺, Ni²⁺, and Cu²⁺) are loaded.²⁶ Surface modification of carbon nitride to manipulate the oxygen activation pathway seems to be a promising strategy for ROS regulation.²⁷ For instance, the modification of carbon nitride with C-O-C, C-O, NO₂, and C=O as surface groups can enhance ¹O₂ generation and suppress the production of H₂O₂ and ·OH.⁷ However, the role of functional groups and the harsh preparation conditions using reflux treatment with concentrated sulfuric/nitric acid limit its application. To date, there is no report on controlling ROS evolution with carbon nitride and then promoting the selectivity of styrene oxide. Thus, it is significantly important in seeking an eco-friendly approach to introduce suitable surface groups to regulate ROS evolution and uncover the reaction mechanism simultaneously.

Herein, we report a simple and environmentally friendly method to introduce a surface cyano group onto carbon nitride by co-pyrolyzing trithiocyanuric acid with thiourea (Figure 1A). The cyano-group-modified samples CNCY and CN-T have special spatial structures that can control the transfer of oxygen and inhibit the generation of H₂O₂ or ·OH, achieving a higher styrene oxide yield than the cyano-free sample. The ¹³C NMR spectrum reveals that the cyano groups bond with the intact heptazine ring. And this unique structure reduces the steric resistance of styrene as attacking the adsorbed ¹O₂ or -O-O-, which could inhibit the side reaction pathway and prompt the formation of epoxy products. Various characterization techniques and density functional theory (DFT) calculations were used to investigate the reaction mechanism. During the pyrolysis of thiourea, the generated SCN⁻ species^{28,29} react with the terminal -NH₂ forming -C≡N groups, which is the same as the thiocyanuric acid pyrolysis process reported before.^{4,30} Compared with the traditional method whereby excessive thiocyanate (KSCN, NaSCN, etc.) (Scheme S1) is added, this novel strategy with cyano group introduction avoids using alkali-metal ions.³¹ This is the first report on the use of thiourea as the cyano group precursor, aimed at preparing a unique space configuration and in turn controlling the ROS evolution. Other precursors, such as dicyandiamide or melamine, are also applicable, which opens broader application of our strategy for cyano group introduction.

Oxidation of styrene



Oxygen activation



Scheme 1. Proposed Reaction Pathways for the Oxidation of Styrene (Equations 1 and 2) and Oxygen Activation (Equations 3, 4, 5, 6, 7, 8, 9, and 10)

RESULTS AND DISCUSSION

Crystal Structure Changes after Cyano Group Modification and Correlation with the Selectivity Control

The X-ray diffraction (XRD) patterns of cyano-group-modified samples CNCY (prepared using trithiocyanuric as precursor) and CN-T (prepared using trithiocyanuric and thiourea as precursors) show a weaker in-plane peak (100) at 12.8° and interlayer stacking (002) peak at 27.5° compared with those of the cyano-free sample CN (prepared using melamine as precursor) (Figure 1B),^{32,33} indicating decreased crystallinity after cyano group introduction. The morphology of CN, CNCY, and CN-T was analyzed by scanning electron microscopy (SEM) and transmission electron microscopy (TEM). As shown in Figures S3 and S4, a porous and sheet-like morphology is observed after cyano group introduction. The specific surface area and pore volume of CNCY and CN-T are similar (Figure S5 and Table S2), and are larger than those of the CN sample, in turn providing more active sites and promoting the catalytic reaction.³³

The molecular structure change of the samples was studied by Fourier transform infrared (FTIR) spectroscopy. Compared with the CN sample, a new peak around 2,100–2,250 cm^{-1} , which can be identified as the cyano group,³¹ was observed for CNCY and CN-T. The peak area of the cyano group increases with thiourea addition; however, excessive thiourea will decrease the peak area of the cyano group (Figure 1C). The controlled sample CN_{th} with thiourea as precursor was then prepared, yet exhibits low cyano peak intensity in the FTIR spectroscopy (Figure S6). We speculate that superfluous SCN⁻ fragments from pyrolysis with thiourea will polymerize with each other. Thus, the cyano group can be introduced only by maintaining the appropriate concentration of SCN⁻ fragments in the polymerization process.

The chemical composition and structure of the obtained cyano-group-modified samples were studied by X-ray photoelectron spectroscopy (XPS). The presence of N 1s and C 1s signals of CNCY and CN-T samples indicates the successful introduction of a cyano group in the heptazine. The three peaks centered at 398.6, 400.1, and 401.3 eV (Figure 1D) are attributed to the C-N=C, N-(C)₃, and C-N-H_x groups in the heptazine framework, respectively.³⁴ The relative peak area ratios of C-N-H with the total area decrease from 3.8% to 3.4% and 3.0% (calculation method is shown in Table S3) for CN, CNCY, and CN-T samples, respectively, indicating that some C-N-H groups were replaced. It has been reported that the C 1s binding energy of

-C≡N at 286.4 eV is similar to that of C-NH_x, and the introduction of cyano groups led to the generation of amino (-NH₂) groups and an enhanced peak intensity at 286.4 eV.³⁵ However, there is no obvious enhancement in the peak area (Figure 1E) and the peak area ratios between C-NH_x and -C≡N and the N-C=N of the three samples were all 0.03 (calculation method is shown in Table S4). These results demonstrate that the cyano group is introduced by replacing the C-N-H groups, while the structure of heptazine remains unchanged. In addition, the absence of sulfur signal (Figure S7) in CNCY and CN-T indicates that all the sulfurs are removed from the samples.

Figure S8 gives the solid-state ¹³C NMR spectra of CN, CNCY, and CN-T. It can be seen that all samples present two strong signal groups at 156.2 and 164.3 ppm, corresponding to the C(1) atoms of N=C-N(NH_x) and the C(3 or 5) atoms of N=C-N₂ in the heptazine units, respectively.³⁶ For CN-T, two new peaks at 123.5 and 162.6 ppm can also be clearly observed, which can be assigned to the C(17) atoms of -C≡N groups and the neighbor C(1') atoms, respectively. In heptazine, the C(1') atoms at 162.6 ppm are linked to the terminal -NH₂ groups.³⁷ It has been reported that a large number of hydrogen bonds exist between the strands of polymeric carbon nitride units,³⁴ and these hydrogen bonds will passivate the NMR peak type. The -NH-C≡N could break the hydrogen bond structure, leading to the emergence of a sharp peak at 162.6 ppm. Therefore, we can safely conclude that the -C≡N group was bonded with the intact heptazine. As we reported previously, the cyano group content can be obtained by titration (Figure S9 and Table S5; the detailed methods are shown in the Supplemental information).³⁰ A good linear relationship between the cyano group content and the yield of styrene oxide was found (Figure 2A), indicating that cyano groups probably act as the active sites in this reaction. The content of cyano carbon in CN-T is only 0.83 wt% based on the cyano group content (1.8 wt%), which might explain its low signal intensity in ¹³C NMR spectra.

Structure-Activity Relationship after Cyano Group Introduction

The results from various temperatures, light intensities, and wavelengths indicate that the epoxidation of styrene is primarily driven by photoinduced electrons (Figures S10 and S11). For semiconductor photocatalysis, the generation and separation efficiency of photogenerated carriers can directly affect the catalytic performance.³⁸ The transient photocurrent, electrochemical impedance spectroscopy, steady-state photoluminescence (PL), and time-resolved PL spectra results all demonstrate that the recombination efficiency of charge carriers for the cyano-modified sample is lower than for the bulk carbon nitride (Figure S12). Yet, in our system, the improvement of charge separation efficiency shows no influence on the selectivity of the products.

In the dynamic experiments, there is only a slight change in the styrene oxide selectivity over CN and CN-T as the reaction is prolonged. Furthermore, at the same conversion rate, CN-T shows higher styrene oxide selectivity than the cyano-free sample (Figure 2B). These results indicate that the selectivity is mainly dependent on the structure of active sites (major factor) rather than the enhancement of photoelectric performance (minor factor). The photoelectric performance of carbon nitride can be significantly improved by heteroatom doping, such as with phosphorus, without changing the terminal group of the sample.³⁹ In the controlled experiment, the phosphorus-doped sample CN-P (prepared using melamine as precursor and 0.25 g ammonium phosphate as doping source), which shows better photoelectric performance than CN, was prepared and investigated (Figure S13A and Table S6). The conversion of styrene was increased, whereas the selectivity of styrene oxide was not improved. Furthermore, CNMT (prepared using 10 g melamine mixed with 0.3 g thiourea as precursor) and CNDT (prepared using 10 g dicyandiamide mixed with 0.3 g thiourea as precursor) were prepared. These samples show higher cyano peak area in the FTIR spectra and better catalytic performance and selectivity for styrene oxide than bulk carbon nitride (CN and CND) (Figure S13). These results further confirm that the cyano group could improve the selectivity of the styrene oxide product.

The band structures of the catalysts were studied and determined by combining the results of UV-Vis spectra, Kubelka-Munk formula, and Mott-Schottky electrochemical test (Figure S14). The CB and VB positions of all

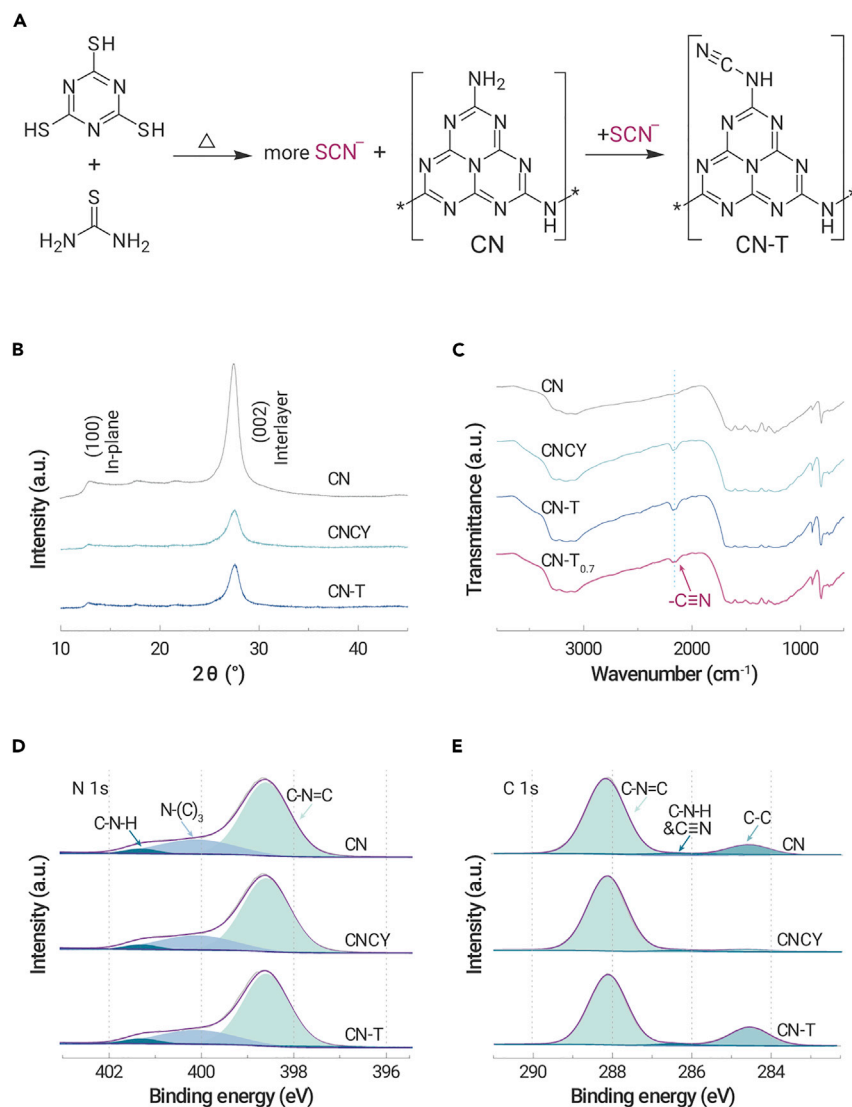


Figure 1. Structure Characterization of Cyano-Group-Modified Carbon Nitride (A) Proposed cyano introduction mechanism via trithiocyanuric acid and thiourea co-polymerization.

(B) XRD patterns of CN, CNCY, and CN-T.

(C) FTIR spectra of CN, CNCY, CN-T, and CN-T_{0.7}.

(D and E) N 1s and (E) C 1s XPS spectra of CN, CNCY, and CN-T.

samples make them able to activate O₂ forming O₂^{•-} species (Scheme 1, Equation 3), whereas they are unable to directly oxidize water to [•]OH (Equation 7) (Figure 3A).⁴⁰ Electron paramagnetic resonance (EPR) is a powerful technique to monitor catalytically relevant species that contain unpaired electrons.⁴¹ The *in situ* EPR spectra in Figure 3B show that the [•]OH signal intensity²⁷ is the highest for the CN sample and reduces with the increase in cyano group content in CNCY_x and CN-T. It is probable that the [•]OH is formed through the decomposition of H₂O₂ as follows from Equation 5. The content of H₂O₂ decreases as the cyano groups increase and a trace of H₂O₂ was detected for CNCY or CN-T (Figure S15; the H₂O₂ content was determined by iodometry as shown in the Supplemental information). These results indicate that the introduced cyano groups successfully inhibit the generation of H₂O₂ and [•]OH species, while O₂^{•-}, ¹O₂, and -O-O- species are probably the main ROS that participate in the epoxidation reaction.

To identify the individual role of ROS involved in this study, O₂^{•-} and ¹O₂ scavengers were adopted in the reaction system. The reaction was completely terminated after adding 0.05 eq of tetrazolium blue (NBT, O₂^{•-} scavenger, the dosage is comparable to styrene)⁴ (Figure S16A). Meanwhile, the conversion rate (Figure S16B) dropped by 45% after adding 9,10-diphenylanthracene⁴² as a ¹O₂ trapping agent. This indicates that O₂^{•-} is the initial active species that can convert to other ROS. In general, ¹O₂ is generated through an energy transfer process from the excited carbon nitride via dipole-dipole (Förster processes) or direct electron-exchange interactions

(Dexter processes).⁴³ Adding NBT can terminate the whole reaction, which indicates that ¹O₂ is formed via the O₂^{•-} oxidation process (Equation 10) rather than a conventional energy transfer process.⁸ We speculate that this transformation path improves the utilization of photogenerated charge carriers, because it consumes electrons and holes subsequently. Only 27% of ¹O₂ is observed with the cyano-free sample, which illustrates the low utilization efficiency of photogenerated charge carriers. As previously reported, O₂^{•-} could be adsorbed on the surface of carbon nitride and reduced to -O-O- through a fast two-electron reduction reaction.^{23,24} Thus the remaining 55% of O₂^{•-} in the cyano-group-modified sample probably evolves into -O-O- species.

The formation of -O-O- species and the function of cyano groups in this process were confirmed by *in situ* FTIR spectra measurements. Under illumination, the cyano-group-modified sample exhibits a clear vibration peak around 892 cm⁻¹ (-O-O-)^{23,44,45} under an oxygen atmosphere (Figure 3C). Meanwhile, the intensity of the cyano group increases gradually with the above peak (Figure 3D, bottom), which can be attributed to the electron transfer between the O₂ and the cyano group and the change in dipole moment of the cyano group.^{25,46} The role of the cyano group as an oxygen transformation site is confirmed by adding 20 μL of styrene into the reaction cell. In the first 20 min, the intensity of the cyano group remains almost unchanged, yet the twisted vibration (990 cm⁻¹) and out-of-plane oscillation (910 cm⁻¹) of =CH₂ is decreasing (Figure 3E).⁴⁷ As time goes on, the intensity of the cyano groups increases (Figure 3D, top) with the increase in the -O-O-

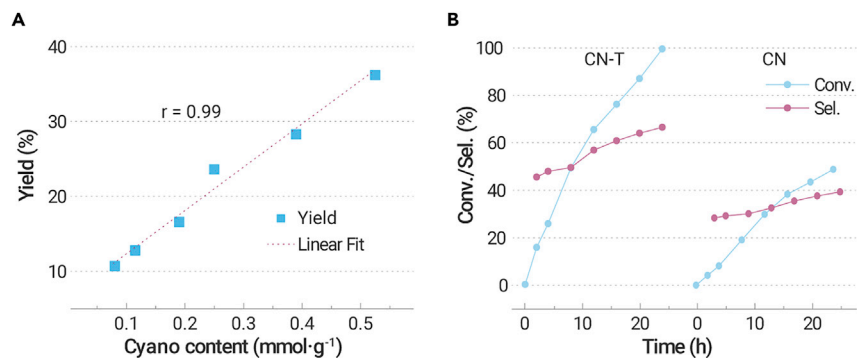


Figure 2. Catalytic Performance Test of Cyano-Group-Modified Carbon Nitride (A) Styrene oxide yield as a function of cyano content.

(B) Time profile of the conversion and the selectivity of styrene oxide over CN-T and CN. Reaction conditions: 0.04 mmol of styrene, 2 mL of acetonitrile, 10 mg of catalyst, 1 atm air, 400 mW/cm² white LED light irradiation, 60 °C, 4 h (for A) and 12 h (for B). Conv., conversion; Sel., selectivity for styrene oxide.

(890 cm⁻¹) vibration peak (Figure 3E). These results indicate that the cyano group is the active site for ROS evolution, which could anchor the -O-O- and then facilitate the attack of styrene. The interaction between ¹O₂ and the cyano groups was studied by DFT calculation. In the cyano-free sample, according to the work reported and our calculation results, ¹O₂ also prefers to be adsorbed at the N4-C1 site (Figure S17 and Table S7).²⁴ However, the optimized configuration was changed after cyano modification. As shown in Figure 3F, (i) and (ii) are more stable than the other five configurations (Fig-

ure S18 and Table S8). This indicates that the interaction of ¹O₂ with a cyano-group-modified sample is the strongest when the ¹O₂ is located at the N7-C17 (Figure 3F, i) or N7-N18 (Figure 3F, ii) site with a relative energy of -39.3 and -39.1 kJ/mol, respectively. It is only -28.6 kJ/mol when the ¹O₂ is located at N4-C1.

According to the above analysis, we can safely conclude that the cyano groups bond with the heptazine ring and act as the optimal adsorption site for -O-O- and ¹O₂ species. This unique configuration will change the reaction

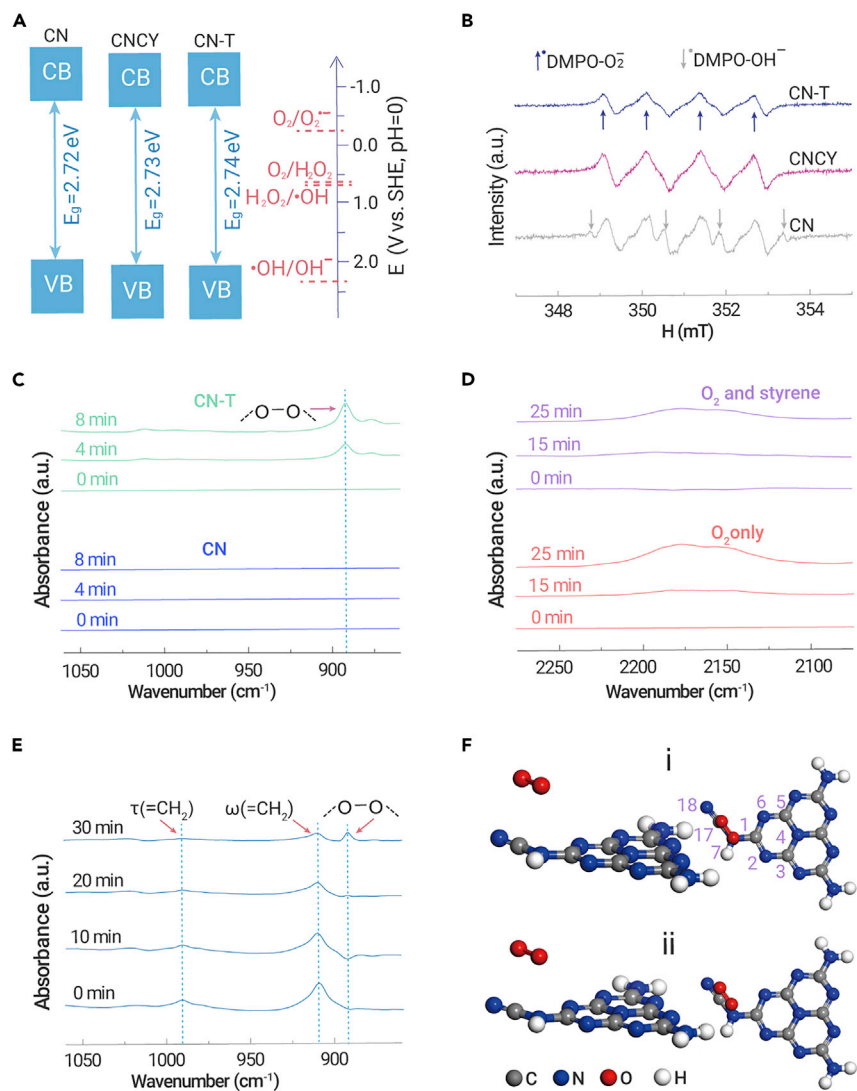
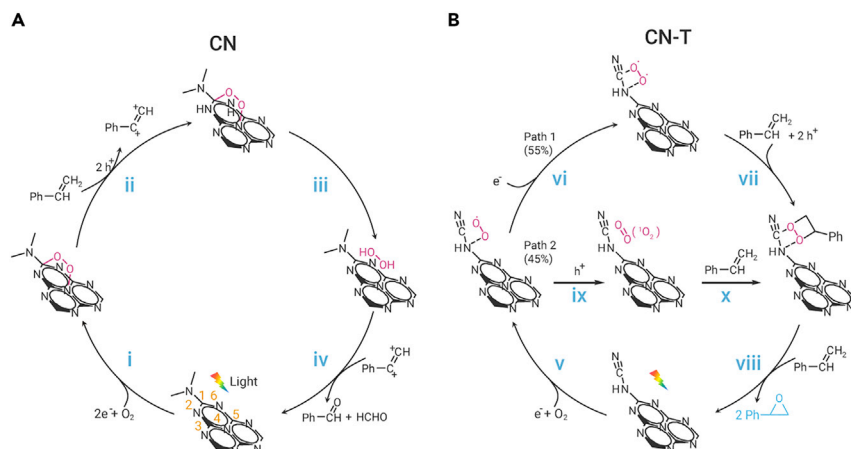


Figure 3. Characterization of Reactive Oxygen Species (A) Band structure of CN, CNCY, and CN-T.

(B) *In situ* EPR spectra. Room-temperature EPR spectra were measured after *in situ* illumination for 5 min by using DMPO as trap agent.

(C-E) *In situ* FTIR spectra of CN-T with the addition of O₂ or dual addition of O₂ and styrene to observe the formation of ROS (peroxy species) and the reaction pathway on the catalyst surface. The FTIR spectra were obtained in a sealed *in situ* reaction cell and the dosages of the styrene and oxygen were 20 μL and 5 mL (1 atm), respectively.

(F) Dioxigen adsorption mode on cyano-modified sample, located above (i) N7-C17 or (ii) N7-N18.



Scheme 2. Proposed Reaction Mechanism for Epoxidation of Styrene over Cyano-Group-Free and Cyano-Group-Modified Carbon Nitride

pathway. Traditionally, the $-O-O-$ and 1O_2 species are easily adsorbed at C1-N4 (inset of Figure 3F) in the cyano-free sample CN.²⁴ However, owing to the steric hindrance caused by the rigid plane heptazine ring units, it is difficult for the activated styrene to attack the $-O-O-$ or 1O_2 species at C1-N4. Furthermore, the 1,4-adsorption mode of $-O-O-$ (i–iii in Scheme 2) in cyano-free CN is favorable for the attack of protons (at positions 2 and 6) forming H_2O_2 .⁵ Once the $-O-O-$ and 1O_2 are adsorbed at the cyano group site, the steric hindrance will be drastically reduced, which will be beneficial for generating olefin oxidation intermediates. Meanwhile, after cyano group introduction, the terminal adsorption mode formed will increase the offensive distance of protons to form H_2O_2 , and also provide a retrospective interpretation of why a trace of H_2O_2 was detected with cyano-group-modified carbon nitride. Thus, the cyano groups bonded with the heptazine ring (structure B, Table 1) is favorable for enhancing the influence of spatial configuration on product selectivity. For comparison, cyano-group-modified carbon nitrides with different spatial configurations were prepared (structures C and D, post-heating treat-

ment,⁴⁸ copolymerization with NaCl,⁴⁹ KOH etching³⁵ and post-treatment using $NaBH_4$,⁵⁰ structure B, KSCN coheating³¹). As shown in Table 1, only the samples with B-type structure can increase the yield of styrene oxide. This demonstrates that the spatial configuration determines the reaction selectivity.

Catalyst Stability and Reaction Scale-up under Solar Irradiation

These cyano-group-modified samples exhibit high stability. There is no obvious change in XRD, UV, or FTIR spectra after recycling five times (Figures S19A–S19C). The yield of styrene oxide remains unchanged above 65% (Figure S19D, diamond), which is superior to the catalytic performance of iron, cobalt-based, and zeolites (summarized in Table S1). With isobutyraldehyde as reductant the yield of styrene oxide further increases to 85% (Figure S19D, star), since the isobutyraldehyde can promote the conversion of the olefin oxidation intermediate to the styrene oxide products.¹⁰ As shown in Table

Table 1. Photocatalytic Activity over Various Carbon Nitride Catalysts under Visible Light^a

Entry	Sample	Yield (%)	Sample structure	Reference
1	CN	19.2	A	this paper
2	CN-T	65.7↑	B	this paper
3	CN(KSCN)	61.3↑	B	Lau et al. ³¹
4	CN	26.4	A	Niu et al. ⁴⁸
5	CNQ680	23.7	C	Niu et al. ⁴⁸
6	Bulk $g-C_3N_4$	32.3	A	Yuan et al. ⁴⁹
7	Ribbon-like $g-C_3N_4$	15.9	C	Yuan et al. ⁴⁹
8	$g-C_3N_4$	36.5	A	Yu et al. ³⁵
9	$g-C_3N_4$ -0.01	35.1	C	Yu et al. ³⁵
10	CN	20.3	A	Liu et al. ⁵⁰
11	DCN-200	20.1	D	Liu et al. ⁵⁰

^aThe reaction conditions were as follows: 0.04 mmol of styrene, 2 mL of acetonitrile, 10 mg of catalyst, 1 atm air, 400 mW/cm² white LED light irradiation, 60°C, 24 h. Samples in entries 3–11 were synthesized referring to the literature methods (details shown in the Supplemental information).

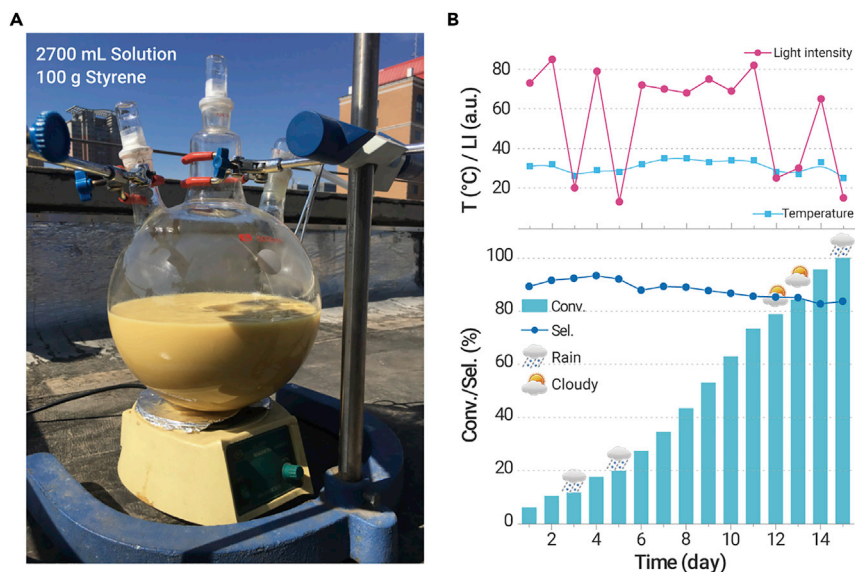


Figure 4. Characterization of Catalytic Performance under Solar Light Irradiation (A) Photograph of up-scaled reaction with volume of 2.7 L.

(B) Amplification reaction with 100 g styrene and the temperature and light intensity change curve. Catalytic setup was placed on a rooftop (latitude 37°51' north, longitude 112°32' east) so that the reactor would be directly irradiated by the sun for the duration of the experiment. Reaction conditions: 100 g of styrene, 2,500 mL of acetonitrile, 200 mL of isobutyraldehyde, 10 g of catalyst, bubble with 1.5 L of oxygen every day, May 28 to June 11, 2020, 25 °C–35 °C, light intensity 13–85 mW/cm². Conv., conversion; Sel., selectivity.

S9, the cyano-group-modified photocatalyst also exhibits good performance on electron-rich group-containing, aromatic, conjugated, and linear alkenes.

The scale-up reaction driven by solar light was conducted to investigate the performance of the catalyst for industrial application. Figure 4 depicts the scaled-up reaction (styrene was up to 100 g, which was 25,000-fold quality increase compared with the lab-scale reactions) under solar light irradiation. The reaction temperature and solar light intensity ranged from 25 °C to 35 °C and 13 to 85 mW/cm², respectively. The conversion rate could reach above 99% with a selectivity of >82% in the scaled-up reaction under identical irradiation time (Figure 4B). It should be noted that the conversion rate will decrease on rainy or cloudy days; this result implies that it will be easier to realize the practical application of photocatalysis in drought areas or those with long sunshine time.

Based on the above discussion, a possible mechanism is proposed (Scheme 2). The catalyst has an appropriate CB position to activate oxygen forming O₂^{•−}, of which 45% could convert to ¹O₂. The ¹O₂ is preferentially adsorbed on the cyano group, facilitating the attack of styrene. The remaining 55% of the O₂^{•−} can convert to -O-O- via a fast two-electron reduction process, and the -O-O- could also be adsorbed on the cyano group. The styrene is more easily absorbed in the hole-enriched region, such as 2 and 6 in Scheme 2A,²⁴ and transfer an electron to the VB of the catalyst. The activated styrene will react with the -O-O- or ¹O₂ to generate a four-membered ring intermediate. In the action of another styrene molecule, two molecules of styrene oxide are finally formed. This process is similar to the transition-metal activation process discussed in the introduction, which can avoid the bond-breaking reaction and then increase the selectivity of styrene oxide.

CONCLUSIONS

In conclusion, we successfully designed and synthesized cyano-group-modified carbon nitrides CNCY_x and CN-T_y for selective epoxidation of styrene. The cyano-group-modified sample achieved higher styrene yield than the bulk carbon nitride using O₂ as oxidant. Solid-state ¹³C NMR and XPS spectra proved that the cyano group bonded with the heptazine ring. The *in situ* FTIR spectra and DFT calculations demonstrated that cyano groups could selectively adsorb peroxy and ¹O₂ species. This structure could also inhibit the formation of H₂O₂ and [•]OH species as well as reducing the steric hindrance beneficial to the interaction between the active site and styrene. Thus, the special spatial structure, which could adjust the transformation of ROS, led to the enhanced photocatalytic epoxidation of styrene for cyano-group-modified carbon nitride. The cyano-group-modified sample can be applied to a variety of substrates and the catalytic system can be scaled up to 2.7 L under solar irradiation. This surface-group-modification

strategy highlights that a surface-functionalized carbon nitride photocatalyst could be prepared via a simple and green route, which opens up a new window to design and fabrication of highly active metal-free photocatalysts for solar ray-driven selective controlled organic synthesis.

MATERIALS AND METHODS

Materials

All chemicals were purchased from Aladdin and used as received without further purification.

Catalyst Preparation

Cyano-Modified Samples (CN-T_y). Typically, *y* g (*y* = 0.1, 0.3, 0.5, and 0.7) of thiourea and 10 g of trithiocyanuric acid were dissolved in 100 mL of deionized water under vigorous stirring. The deionized water was evaporated at 95 °C to afford a yellow block mixture powder. The mixture powder was collected and heated in a crucible loaded in a muffle furnace at 550 °C for 4 h with a ramp rate of 3 °C/min. The samples were named as CN-T_y. The CN-T_{0.3} sample showed highest catalytic performance (Figure S1) and was also named as **CN-T**.

Cyano-Modified Samples (CNCY_x). The samples were prepared by the thermal polymerization method as we reported previously.⁴ Typically, *m* g of melamine and *n* g of trithiocyanuric acid (*m* + *n* = 10, *x* = *n*/(*m* + *n*)) were dissolved in 50 mL of deionized water under vigorous stirring. The deionized water was evaporated at 95 °C to afford a yellow block mixture powder. After that the mixture powder was treated following the above calcination procedure. Among the samples, CNCY_{1.00} exhibited the highest catalytic performance in the epoxidation reaction and was abbreviated as **CNCY** (Figure S1).

Bulk Carbon Nitride (CN). The bulk carbon nitride was prepared by using melamine as precursor, following the above calcination procedure. The sample was named as CN. Other samples mentioned in this study were prepared by the reported methods (details shown in the Supplemental information).

The above light-yellow product was ground thoroughly into a fine powder using a pestle and mortar prior to various characterizations.

Structural Characterization

Powder XRD patterns were collected using a Bruker D8 Advanced diffractometer operating with a Cu Kα X-ray source (λ = 1.5405 Å). The scan range was from 5° to 60° with the scan rate of 5°/min. FTIR spectra were obtained by a Bruker Tensor II spectrometer in a KBr pellet and the frequency range was 4,000–600 cm^{−1}. SEM was performed using a Hitachi S-4800 microscope with an acceleration voltage of 5 kV. Morphology was assayed using TEM (Technai G2 F20 S-Twin) with an accelerating voltage of 200 kV. The specific surface areas were analyzed by a nitrogen adsorption-desorption instrument (TriStar II 3020). Prior to measurement, all the photocatalysts were degassed under evacuation at 120 °C for 10 h. The pore size distribution was obtained by desorption isotherms using the Barret-Joyner-Halenda method. UV-Vis diffuse reflectance spectra were obtained on a Shimadzu UV 3600 spectrophotometer using BaSO₄ as the reference. XPS was conducted on a USA Thermo ESCALAB 250 spectrometer using a monochromate Al Kα X-ray radiation source (200 W). The binding energy correction was referenced to C 1s peak (284.6 eV) arising from surface

hydrocarbons. The spectra deconvolution was carried out using the XPS PEAK41 software package. The solid NMR spectra were performed using a Bruker AV-III 600 MHz wide-bore spectrometer equipped with a 4 mm double-resonance probe. Steady-state PL spectra were performed on a Hitachi F-7000 FL spectrophotometer at room temperature with an excitation wavelength of 365 nm. Time-resolved PL decay curves were recorded on a FLS920 fluorescence lifetime spectrophotometer (Edinburgh Instruments, UK) under excitation of 365 nm and probed at 460 nm. EPR measurements were obtained using a Bruker model EMXPLUS 10/12 spectrometer. The samples were prepared as follows: 1 mg of the catalyst was dispersed in 1 mL of acetonitrile by sonication; 10 μ L of the above mixture was mixed with 10 μ L of DMPO acetonitrile solution (1 mg/ μ L). The EPR spectra were measured after *in situ* illumination for 5 min. The *in situ* diffuse reflectance infrared experiments were performed on Bruker Tensor II FTIR spectrometer (Figure S2).

REFERENCES

- Lin, Y., Pan, X., Qi, W., et al. (2014). Nitrogen-doped onion-like carbon: a novel and efficient metal-free catalyst for epoxidation reaction. *J. Mater. Chem. A* **2**, 12475–12483, <https://doi.org/10.1039/C4TA01611D>.
- Almassmy, Y.A., and Pescarmona, P.P. (2019). The role of water revisited and enhanced: a sustainable catalytic system for the conversion of CO₂ into cyclic carbonates under mild conditions. *ChemSusChem* **12**, 3856–3863, <https://doi.org/10.1002/cssc.201901124>.
- Hu, T.D., Jiang, Y., and Ding, Y.H. (2019). Computational screening of metal-substituted HKUST-1 catalysts for chemical fixation of carbon dioxide into epoxides. *J. Mater. Chem. A* **7**, 14825–14834, <https://doi.org/10.1039/c9ta02455g>.
- Tan, H., Gu, X., Kong, P., et al. (2019). Cyano group modified carbon nitride with enhanced photoactivity for selective oxidation of benzylamine. *Appl. Catal. B. Environ.* **242**, 67–75, <https://doi.org/10.1016/j.apcatb.2018.09.084>.
- Kofuji, Y., Isobe, Y., Shiraiishi, Y., et al. (2016). Carbon nitride–aromatic diimide–graphene nanohybrids: metal-free photocatalysts for solar-to-hydrogen peroxide energy conversion with 0.2% efficiency. *J. Am. Chem. Soc.* **138**, 10019–10025, <https://doi.org/10.1021/jacs.6b05806>.
- Cui, Y., Ding, Z., Liu, P., et al. (2012). Metal-free activation of H₂O₂ by g-C₃N₄ under visible light irradiation for the degradation of organic pollutants. *Phys. Chem. Chem. Phys.* **14**, 1455–1462, <https://doi.org/10.1039/C1CP22820J>.
- Wang, H., Jiang, S., Chen, S., et al. (2016). Enhanced singlet oxygen generation in oxidized graphitic carbon nitride for organic synthesis. *Adv. Mater.* **28**, 6940–6945, <https://doi.org/10.1002/adma.201601413>.
- Nosaka, Y., and Nosaka, A.Y. (2017). Generation and detection of reactive oxygen species in photocatalysis. *Chem. Rev.* **117**, 11302–11336, <https://doi.org/10.1021/acs.chemrev.7b00161>.
- Al-Ajlouni, A.M., and Espenson, J.H. (1995). Epoxidation of styrenes by hydrogen peroxide as catalyzed by methylrhodium trioxide. *J. Am. Chem. Soc.* **117**, 9243–9250, <https://doi.org/10.1021/ja00141a016>.
- Frimer, A.A. (1979). The reaction of singlet oxygen with olefins: the question of mechanism. *Chem. Rev.* **79**, 359–387, <https://doi.org/10.1021/cr60321a001>.
- Barak, G., and Sasson, Y. (1987). Dual-function phase-transfer catalysis in the metal-assisted oxidation by hydrogen peroxide of styrene to benzaldehyde or acetophenone. *J. Chem. Soc. Chem. Commun.* 1266–1267, <https://doi.org/10.1039/C39870001266>.
- Sebastian, J., Jinka, K.M., and Jasra, R.V. (2006). Effect of alkali and alkaline earth metal ions on the catalytic epoxidation of styrene with molecular oxygen using cobalt(II)-Exchanged zeolite X. *J. Catal.* **244**, 208–218, <https://doi.org/10.1016/j.jcat.2006.09.005>.
- Rahman, S., Santra, C., Kumar, R., et al. (2014). Highly active Ga promoted Co-HMS-X catalyst towards styrene epoxidation reaction using molecular O₂. *Appl. Catal. A Gen.* **482**, 61–68, <https://doi.org/10.1016/j.apcata.2014.05.024>.
- Liu, J., Meng, R., Li, J., et al. (2019). Achieving high-performance for catalytic epoxidation of styrene with uniform magnetically separable CoFe₂O₄ nanoparticles. *Appl. Catal. B. Environ.* **254**, 214–222, <https://doi.org/10.1016/j.apcatb.2019.04.083>.
- Caudillo-Flores, U., Munoz-Batista, M.J., Hungria, A.B., et al. (2019). Toluene and styrene photo-oxidation quantum efficiency: comparison between doped and composite tungsten-containing anatase-based photocatalysts. *Appl. Catal. B. Environ.* **245**, 49–61, <https://doi.org/10.1016/j.apcatb.2018.12.032>.
- Huang, Y., Liu, Z., Gao, G., et al. (2017). Stable copper nanoparticle photocatalysts for selective epoxidation of alkenes with visible light. *ACS Catal.* **7**, 4975–4985, <https://doi.org/10.1021/acscatal.7b01180>.
- van Schie, M.M.C.H., Paul, C.E., Arends, I.W.C.E., and Hollmann, F. (2019). Photoenzymatic epoxidation of styrenes. *Chem. Commun.* **55**, 1790–1792, <https://doi.org/10.1039/C8CC08149B>.
- Zheng, Y., Jiao, Y., Chen, J., et al. (2011). Nanoporous graphitic-C₃N₄@Carbon metal-free electrocatalysts for highly efficient oxygen reduction. *J. Am. Chem. Soc.* **133**, 20116–20119, <https://doi.org/10.1021/ja209206c>.
- Deng, X., Cao, H., Chen, C., et al. (2019). Organotellurium catalysis-enabled utilization of molecular oxygen as oxidant for oxidative deoxygenation reactions under solvent-free conditions. *Sci. Bull.* **64**, 1280–1284, <https://doi.org/10.1016/j.scib.2019.07.007>.
- Xiong, X., Wang, Z., Zhang, Y., et al. (2020). Wettability controlled photocatalytic reactive oxygen generation and Klebsiella pneumoniae inactivation over triphase systems. *Appl. Catal. B. Environ.* **264**, 118518, <https://doi.org/10.1016/j.apcatb.2019.118518>.
- Wang, X., Zhou, C., Shi, R., et al. (2019). Supramolecular precursor strategy for the synthesis of holey graphitic carbon nitride nanotubes with enhanced photocatalytic hydrogen evolution performance. *Nano Res.* **12**, 2385–2389, <https://doi.org/10.1007/s12274-019-2357-0>.
- Wang, Z.-T., Xu, J.-L., Zhou, H., and Zhang, X. (2019). Facile synthesis of Zn(II)-doped g-C₃N₄ and their enhanced photocatalytic activity under visible light irradiation. *Rare Met.* **38**, 459–467, <https://doi.org/10.1007/s12598-019-01222-5>.
- Shiraiishi, Y., Kanazawa, S., Kofuji, Y., et al. (2014). Sunlight-driven hydrogen peroxide production from water and molecular oxygen by metal-free photocatalysts. *Angew. Chem. Int. Ed.* **53**, 13454–13459, <https://doi.org/10.1002/anie.201407938>.
- Shiraiishi, Y., Kofuji, Y., Sakamoto, H., et al. (2015). Effects of surface defects on photocatalytic H₂O₂ production by mesoporous graphitic carbon nitride under visible light irradiation. *ACS Catal.* **5**, 3058–3066, <https://doi.org/10.1021/acscatal.5b00408>.
- Liu, M., Gao, M., Pei, L., et al. (2021). Tailoring phenol photomineralization pathway over polymeric carbon nitride with cyano group multifunctional active sites. *Appl. Catal. B. Environ.* **284**, 119710–119717, <https://doi.org/10.1016/j.apcatb.2020.119710>.
- Ding, Z., Chen, X., Antonietti, M., and Wang, X. (2011). Synthesis of transition metal-modified carbon nitride polymers for selective hydrocarbon oxidation. *ChemSusChem* **4**, 274–281, <https://doi.org/10.1002/cssc.201000149>.
- Xu, S., Zhou, P., Zhang, Z., et al. (2017). Selective oxidation of 5-hydroxymethylfurfural to 2,5-furandicarboxylic acid using O₂ and a photocatalyst of Co-thiophosphazine bonded to g-C₃N₄. *J. Am. Chem. Soc.* **139**, 14775–14782, <https://doi.org/10.1021/jacs.7b08861>.
- Wang, S., Gao, Q.Y., and Wang, J.C. (2005). Thermodynamic analysis of decomposition of thiourea and thiourea oxides. *J. Phys. Chem. B* **109**, 17281–17289, <https://doi.org/10.1021/jp051620v>.
- Zhang, G., Zhang, J., Zhang, M., and Wang, X. (2012). Polycondensation of thiourea into carbon nitride semiconductors as visible light photocatalysts. *J. Mater. Chem.* **22**, 8083–8091, <https://doi.org/10.1039/c2jm00097k>.
- Tan, H., Kong, P., Liu, M., et al. (2019). Enhanced photocatalytic hydrogen production from aqueous-phase methanol reforming over cyano-carboxylic bifunctionally-modified carbon nitride. *Chem. Commun.* **55**, 12503–12506, <https://doi.org/10.1039/C9CC06600D>.
- Lau, V.W.H., Moudrakovski, I., Botari, T., et al. (2016). Rational design of carbon nitride photocatalysts by identification of cyanamide defects as catalytically relevant sites. *Nat. Commun.* **7**, 12165–12174, <https://doi.org/10.1038/ncomms12165>. <https://www.nature.com/articles/ncomms12165#supplementary-information>.
- Ruan, L.-W., Zhu, Y.-J., Qiu, L.-G., et al. (2014). First principles calculations of the pressure affection to g-C₃N₄. *Comp. Mater. Sci.* **91**, 258–265.
- Cheng, J., Hu, Z., Lv, K., et al. (2018). Drastic promoting the visible photoreactivity of layered carbon nitride by polymerization of dicyandiamide at high pressure. *Appl. Catal. B. Environ.* **232**, 330–339, <https://doi.org/10.1016/j.apcatb.2018.03.066>.
- Kang, Y., Yang, Y., Yin, L.-C., et al. (2015). An amorphous carbon nitride photocatalyst with greatly extended visible-light-responsive range for photocatalytic hydrogen generation. *Adv. Mater.* **27**, 4572–4577, <https://doi.org/10.1002/adma.201501939>.
- Yu, H., Shi, R., Zhao, Y., et al. (2017). Alkali-assisted synthesis of nitrogen deficient graphitic carbon nitride with tunable band structures for efficient visible-light-driven hydrogen evolution. *Adv. Mater.* **29**, 1605148–1605156, <https://doi.org/10.1002/adma.201605148>.
- Zhao, D., Dong, C.-L., Wang, B., et al. (2019). Synergy of dopants and defects in graphitic carbon nitride with exceptionally modulated band structures for efficient photocatalytic oxygen evolution. *Adv. Mater.* **31**, 1903545–1903554, <https://doi.org/10.1002/adma.201903545>.
- Lotsch, B.V., Döblinger, M., Sehnert, J., et al. (2007). Unmasking melon by a complementary approach employing electron diffraction, solid-state NMR spectroscopy, and theoretical calculations—structural characterization of a carbon nitride polymer. *Chem. Eur. J.* **13**, 4969–4980, <https://doi.org/10.1002/chem.200601759>.
- Savateev, A., Ghosh, I., König, B., and Antonietti, M. (2018). Photoredox catalytic organic transformations using heterogeneous carbon nitrides. *Angew. Chem. Int. Ed.* **57**, 15936–15947, <https://doi.org/10.1002/anie.201802472>.
- Guo, S., Deng, Z., Li, M., et al. (2016). Phosphorus-doped carbon nitride tubes with a layered micro-nanostructure for enhanced visible-light photocatalytic hydrogen evolution. *Angew. Chem. Int. Ed.* **55**, 1830–1834, <https://doi.org/10.1002/anie.201508505>.
- Huang, S., Xu, Y., Zhou, T., et al. (2018). Constructing magnetic catalysts with in-situ solid-liquid interfacial photo-fenton-like reaction over Ag₃PO₄@NiFe₂O₄ composites. *Appl. Catal. B. Environ.* **225**, 40–50, <https://doi.org/10.1016/j.apcatb.2017.11.045>.

41. Brückner, A. (2010). In situ electron paramagnetic resonance: a unique tool for analyzing structure–reactivity relationships in heterogeneous catalysis. *Chem. Soc. Rev.* **39**, 4673–4684, <https://doi.org/10.1039/B919541F>.
42. Corey, E.J., and Taylor, W.C. (1964). A study of the peroxidation of organic compounds by externally generated singlet oxygen molecules. *J. Am. Chem. Soc.* **86**, 3881–3882, <https://doi.org/10.1021/ja01072a062>.
43. Kovalev, D., and Fujii, M. (2005). Silicon nanocrystals: photosensitizers for oxygen molecules. *Adv. Mater.* **17**, 2531–2544, <https://doi.org/10.1002/adma.200500328>.
44. Zhang, M., de Respinis, M., and Frei, H. (2014). Time-resolved observations of water oxidation intermediates on a cobalt oxide nanoparticle catalyst. *Nat. Chem.* **6**, 362–367, <https://doi.org/10.1038/nchem.1874>. <https://www.nature.com/articles/nchem.1874#supplementary-information>.
45. Shiraishi, Y., Kanazawa, S., Sugano, Y., et al. (2014). Highly selective production of hydrogen peroxide on graphitic carbon nitride (g-C₃N₄) photocatalyst activated by visible light. *ACS Catal.* **4**, 774–780, <https://doi.org/10.1021/cs401208c>.
46. Nicu, V.P., Autschbach, J., and Baerends, E.J. (2009). Enhancement of IR and VCD intensities due to charge transfer. *Phys. Chem. Chem. Phys.* **11**, 1526–1538, <https://doi.org/10.1039/B816151H>.
47. Masson, J.F., Pelletier, L., and Collins, P. (2001). Rapid FTIR method for quantification of styrene-butadiene type copolymers in bitumen. *J. Appl. Polym. Sci.* **79**, 1034–1041, [https://doi.org/10.1002/1097-4628\(20010207\)79:63.3](https://doi.org/10.1002/1097-4628(20010207)79:63.3).
48. Niu, P., Qiao, M., Li, Y., et al. (2018). Distinctive defects engineering in graphitic carbon nitride for greatly extended visible light photocatalytic hydrogen evolution. *Nano Energy* **44**, 73–81, <https://doi.org/10.1016/j.nanoen.2017.11.059>.
49. Yuan, B., Chu, Z., Li, G., et al. (2014). Water-soluble ribbon-like graphitic carbon nitride (g-C₃N₄): green synthesis, self-assembly and unique optical properties. *J. Mater. Chem. C* **2**, 8212–8215, <https://doi.org/10.1039/C4TC01421A>.
50. Liu, G., Zhao, G., Zhou, W., et al. (2016). In situ bond modulation of graphitic carbon nitride to Construct p–n homojunctions for enhanced photocatalytic hydrogen production. *Adv. Funct. Mater.* **26**, 6822–6829, <https://doi.org/10.1002/adfm.201602779>.

ACKNOWLEDGMENTS

This work was supported by the National Natural Science Foundation of China (21773284), the Key Laboratory of Interface Science and Engineering in Advanced Materials, the Ministry of Education (KLISEAM201903), and the Hundred Talents Program of the Chinese Academy of Sciences and Shanxi Province.

DECLARATION OF INTERESTS

The authors declare that they have no conflicts of interest to this work.

SUPPLEMENTAL INFORMATION

Supplemental Information can be found online at <https://doi.org/10.1016/j.xinn.2021.100089>.

The Innovation, Volume 2

Supplemental Information

**Controllable Generation of Reactive Oxygen Species
on Cyano-Group-Modified Carbon Nitride for Selective
Epoxidation of Styrene**

Hao Tan, Peng Kong, Riguang Zhang, Mengting Gao, Meixian Liu, Xianmo Gu, Weifeng Liu, and Zhanfeng Zheng

Supplemental Note: Case Reports

1. Supplemental Methods.

1.1 Bulk CN. Melamine (10 g) was heated in a crucible using a muffle furnace at 550 °C for 4 h, with a ramp rate of 3 K/min under ambient atmosphere. The light-yellow product was ground thoroughly prior to characterization.

1.2 CND, CN_{th}, CNDT and CNMT. The synthetic method for CND and CN_{th} is similar to the above bulk CN, except using dicyandiamide and thiourea as precursor, respectively. CNDT and CNMT sample was prepared by mixing 0.3 g of thiourea with 10 g of dicyandiamide and melamine respectively and then heated in a crucible using a muffle furnace at 550 °C for 4 h, with a ramp rate of 3 K/min under ambient atmosphere.

1.3 CN (KSCN) in Table 1, entry 3. The synthetic method for CN is identical to the above bulk CN. KSCN treated CN was synthesized by thoroughly grounding CN (800 mg) with KSCN (1.6 g, dried at 140 °C in vacuum) and loaded in an alumina boat. In a tube furnace, this mixture was heated under argon to 400 °C at 30 °C/min ramp for 1 h, and then to 500 °C at 30 °C/min ramp for 30 min. The resulting yellow mass was suspended in water and the insoluble product was isolated by centrifugation, washed with copious amount of water and dried at 60 °C in a vacuum oven.¹

1.4 CN and CNQ680 in Table 1, entries 4 and 5. Pristine graphitic carbon nitride was synthesized using thermal polymerization of dicyandiamide (Aldrich, 99%) at 480 °C for 4 h, with the ramping rate of 2 °C/min in a muffle furnace in air. The resultant yellow agglomerates were milled into powder in a mortar (the sample was named as CN). For the quick thermal treatment, a horizontal tube furnace was heated to target temperatures 680 °C and 250 mg of

$g\text{-C}_3\text{N}_4$ was put in an alumina crucible. A stopwatch was started as soon as the alumina crucible was placed at the targeted heating zone. When the watch ran for 5 min, the crucible was fished out as soon as possible and cool down in air. The whole process is carried out in well ventilated space. The resulting products were collected and named as CNQ680.²

1.5 Bulk $g\text{-C}_3\text{N}_4$ and ribbon-like $g\text{-C}_3\text{N}_4$ in Table 1, entries 6 and 7. As a typical procedure, dicyandiamide and NaCl with the mass ratio of 1:1 were mixed and ground to fine powders using a mortar and pestle. Then in nitrogen atmosphere, the fine powders were heated from room temperature to 600 °C at a rate of 19.3 °C/min and kept at 600 °C for 60 min. After cooling to room temperature, 1 g obtained orange sample was grounded, added into 100 mL deionized water and sonicated for 30 min. The dispersion was centrifuged at 4000 rpm for 10 min to obtain a homogenous dispersion. Then the dispersion was freeze-dried, and the target sample was finally obtained. The bulk $g\text{-C}_3\text{N}_4$ was prepared as a reference by heating dicyandiamide using the same heating procedure.³

1.6 $g\text{-C}_3\text{N}_4$ and $g\text{-C}_3\text{N}_4\text{-0.01}$ in Table 1, entries 8 and 9. Pristine $g\text{-C}_3\text{N}_4$ was prepared by urea pyrolysis according to a standard literature method. Briefly, 15 g of urea was calcined at 450 °C in a muffle furnace for 1 h using a heating rate of 10 °C/min. $g\text{-C}_3\text{N}_4\text{-0.01}$ was synthesized as follows: 15 g of urea was dissolved with stirring into aqueous KOH solutions (KOH 0.01 g in 30 mL H₂O), and then the resulting solution evaporated to dryness in an oven at 80 °C overnight. The solid mixtures of urea and KOH were then calcined at 450 °C in a muffle furnace for 4 h using a heating rate of 10 °C/min. Products were denoted as $g\text{-C}_3\text{N}_4\text{-0.01}$. Following synthesis, all samples were washed with water to remove any residual alkali.⁴

1.7 CN and DCN-200 in Table 1, entries 10 and 11. The pristine $g\text{-C}_3\text{N}_4$ was prepared by the commonly used direct thermal polymerization of dicyandiamide at 550 °C for 4 h with a ramping rate of 3 °C/min in air. After cooled naturally, the yellow product was grounded in an agate mortar to obtain a powder sample. To prepare the defect-modified homojunction $g\text{-C}_3\text{N}_4$, the pristine $g\text{-C}_3\text{N}_4$ was fully mixed with NaBH_4 with a weight ratio of 5:1, followed by heating at 200 °C for 30 min. Then the resultant powders were washed with water, HCl, NaOH, and once again with water (washed several times until neutral) to remove all unreacted and potentially detrimental surface species. The products were denoted as DCN-200 °C.⁵

1.8 Cyano hydrolysis method. In typical procedure, 600 mg of the CNCY_x was dispersed in 200 mL of sulphuric acid solution (3 M) and reflux in 80 °C for 2 h, this sample was named as $\text{CNCY}_x\text{-H}$. The resulting yellow mass was suspended in water and the insoluble product was isolated by centrifugation, washed with copious amount of water until the filtrate is neutral and dried at 60 °C in a vacuum oven.

2. Supplemental In situ Diffuse Reflectance Infrared Experiments.

The setup was consisted of the following parts: (i) a Bruker Tensor II FT-IR spectrometer equipped with a MCT detector; (ii) a Praying MantisTM HVC accessory enclosed with a three-window dome; (iii) a HARRICK ATC-024-4 temperature controller; (iv) a cooling water circulating system; (v) a xenon lamp. Highly purity Ar ($25 \text{ mL}\cdot\text{min}^{-1}$) was used as the carrier gas (Figure S2a).

The tests were carried out according to the following procedures. (1) The fresh powder sample was loaded in the *in situ* reaction cell (Figure S2b). (2) After assembling the HVC with a sample into the spectrometer, the system was warmed to 120 °C with the inlet of Ar gas (25

mL·min⁻¹) for 3 h. The temperature was controlled by the ATC controller and cooling water. (3) After the thermal treatment, until the HVC was cooled to 30 °C, 20 µL of the styrene was introduced to the HVC by dripping. (5) The cell was purged by the Ar gas (25 mL·min⁻¹) to clean up the redundant substrates, until the IR signals stable. (6) The outlet of the cell was sealed and additional 5 mL oxygen was injected into the cell through the latex tube which connected with the intake of the cell (Figure S2c). (7) Samples were irradiated by means of a solar light simulator with a xenon lamp. The solar light simulator was equipped with a cut 420 nm filter to remove ultraviolet irradiation. Meanwhile, IR spectra were collected repeatedly every 1 min (Figure S2c).

3. Supplemental Photoactivity Measurements.

The styrene epoxidation reactions were conducted under air atmosphere (1 atm) in a 25 mL round-bottomed Pyrex glass flask with a sealed spigot and a magnetic stirrer (Figure S9). The suspensions were prepared by mixing styrene (0.04 mmol), acetonitrile (2 mL), and catalyst (10 mg) in a reactor equipped with a stirrer bar. The reactor was irradiated using a white LED light (400 mW/cm²) whilst stirring at 60 °C. The product compositions were analyzed and determined by means of an Agilent HP5973 mass spectrometer and Agilent 1260 high efficiency liquid chromatography. The Agilent Series are equipped with a vacuum degasser, a quaternary pump, an auto sampler and a DAD system, connected to Agilent Chem Station software. A C18 column (250×4.6 mm i.d., 5 µm) was used. The flow rate was 1 mL/min. Solvents that constituted the mobile phase were (A) acetonitrile and (B) water with the volume ratio 65:35. The products were also identified by mass spectrometry (GC-MS, Agilent 6890N) coupled with 5973 Mass selective Detector.

4. Supplemental Quantification methods.

The conversion of styrene and the selectivity of styrene oxide, and benzaldehyde were analysed by HPLC by using the external standard method.

5. Supplemental Acidimetric titration of carbon nitride.

The acidic functional groups and the presences of such groups were determined by a neutralization adsorption experiment. Typically, 100 mg (m_1) CNCY_{1.00} and CNCY-H sample were dispersed into 50 g (m_A) of 0.05 mol/L NaHCO₃ aqueous solution, respectively. The resultant mixtures were allowed to equilibrate with magnetic stirring for 6 h. After that, the mixtures were filtered and the filtrate was collected and 20 g (m_{A1}) of the filtrate or 20 g NaHCO₃ aqueous solution (m_{A0}) was pipetted out and back titrated using 0.025 mol/L (C) hydrochloric acid solutions. Recording the volume of hydrochloric acid consumed as V_{A1} and V_{A0} . The concentrations of the NaHCO₃ aqueous solution were calibrated by standard hydrochloric acid. In the controlled reaction 50 g (m_F) water was used to disperse 100 mg (m_2) of the sample. After stirring for 6 h, 10 g filtrate (m_{F1}) was mixed with 25 g NaOH (m_{FC}) aqueous solution (FC mixture) and back titrated using 0.025 mol/L hydrochloric acid solutions to determination of the acidity and alkalinity of the catalyst surface. Recording the volume of hydrochloric acid consumed as V_F . Bromocresol green–methyl red was used as the indicator. The adsorbed base was calculated using the following equation:

$$n_A = \left(V_{A0} * \frac{C}{m_{A0}} - V_{A1} * \frac{C}{m_{A1}} \right) * \frac{m_A}{m_1} + n_F \quad (s1)$$

$$n_F = \left[\left(V_F * C - V_{C0} * \frac{C * m_{FC}}{m_{C0}} \right) / m_{F1} \right] * m_F / m_2 \quad (s2)$$

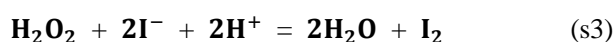
In the equations:

C : Concentration of standard hydrochloric acid (mol/L);

V_{A0} : The hydrochloric acid volume used in calibrating base solution (mL);
 m_{A0} : The quality of base solution used in calibrating by hydrochloric acid (g);
 V_{A1} : The hydrochloric acid volume used in calibrating the above filtrate (mL);
 m_{A1} : The quality of base filtrate solution used in titration (g);
 m_A : The quality of base solution used in sample dispersion (g);
 m_1, m_2 : The consumption quality of our sample (g).
 V_F : The hydrochloric acid volume used in calibrating FC mixture (mL);
 m_{FC} : The quality of FC mixture used in titration (g);
 m_{F1} : 10 g;
 m_F : The quality of water used in sample dispersion (g).

6. Supplemental Quantitative determination of hydrogen peroxide content by iodometry.

The H_2O_2 generated in the reaction were determined by a typical iodometry method. Typically, 2 mL of reaction solution was filtered after illumination for 6 h, then 10 μ L of sulfuric acid solution (1 mL sulphuric acid mixed with 8 mL deionized water) was dropped into the above filtrate. After that, 1 g of KI and 30 μ L of ammonium molybdate (30 g/L) were added in turn, the resultant mixtures were allowed to equilibrate with magnetic stirring for 5 minutes. Finally, the mixtures were titrated using $Na_2S_2O_3$ and Na_2CO_3 mixture solution (25 g/L of $Na_2S_2O_3 \cdot 5H_2O$, 0.2 g/L of Na_2CO_3) until the solution becomes colourless. In the controlled reaction water was used to as the contrast. The reactions between H_2O_2 , I_2 and $Na_2S_2O_3$ were showed as below.



According to the reaction equation the H_2O_2 content is equal with two stoichiometric ratios of

Na₂S₂O₃.

7. Supplemental Photoelectrochemical (PEC) Measurements.

The working electrode was prepared by the drop-casting method. In a typical process, 5 mg of the catalyst powder was mixed with 0.5 g of 2 wt.% polyvinylidene difluoride (PVDF) N-methyl pyrrolidone (NMP) solution by sonication, then 20 μ L of the slurry was dropped onto fluorine-doped tin oxide (FTO, 2 cm \times 1.5 cm) glass electrode through a layer-by-layer method. Photocurrent measurements were performed under LED light illumination conditions in a 0.2 M Na₂SO₄ solution by using the Amperometric it Curve technique with the pH maintained at 6.6. Mott–Schottky plots were also obtained with the working electrodes immersed in 0.2 M Na₂SO₄ aqueous solution, yet, by using the impedance–potential technique.

The potential conversion relation is according to the Nernst equation:

$$E(\text{NHE}) = E(\text{Ag}/\text{AgCl}) + 0.197 \quad (\text{s5})$$

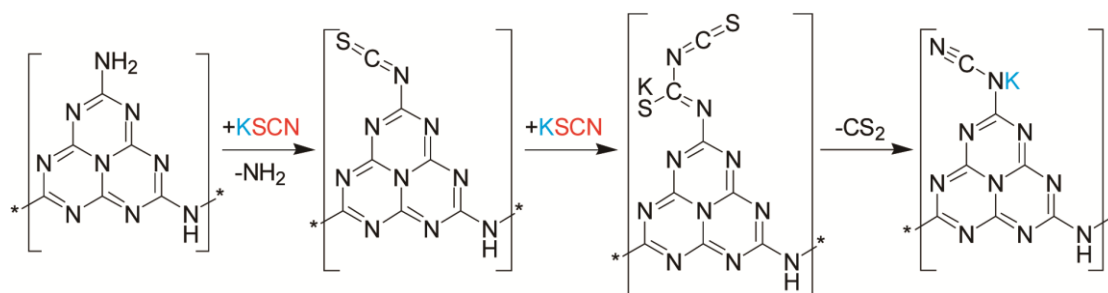
$$E(\text{RHE}) = E(\text{NHE}) + 0.0591 \times \text{pH} \quad (\text{s6})$$

Note: The potential of RHE is related to pH value, when the pH = 0, the potential of RHE is equivalent to SHE.

The electrochemical impedance spectra (EIS) were obtained by using the A. C. Impedance technique. The working electrodes were immersed in mixture aqueous solution. The composition of the mixture solution was as follows: 0.1 mol/L KCl, 2 mmol/L K₃[Fe(CN)₆] and 2 mmol/L K₄Fe(CN)₆·3H₂O. All the above tests were characterized on a workstation (CHI 760D, CH Instruments, Inc., Shanghai, China) in a three–electrode model, with Pt wire as the counter electrode and Ag/AgCl electrode (saturated KCl) as the reference electrode.

8. Supplemental Computational Methods.

All density functional theory calculations (DFT) calculations were implemented in Dmol³ program package of Materials Studio 8.0.^{6, 7} The exchange-correlation functional PBE was used to calculate the electronic structure with generalized gradient approximation (GGA).^{8, 9} The valence electron functions were expanded into a set of numerical atomic orbital by a double numerical basis with polarization functions (DNP).^{10, 11} All atoms were treated with an all-electron basis set. Meth fessel–Paxton smearing of 0.005 Ha was adopted. The dispersion-corrected (DFT-D2) method is used to describe the dispersion interaction. All energies obtained in our calculations included the zero-point vibrational energy



Scheme S1. Proposed cyano introduction mechanism by KSCN assisted synthesis.

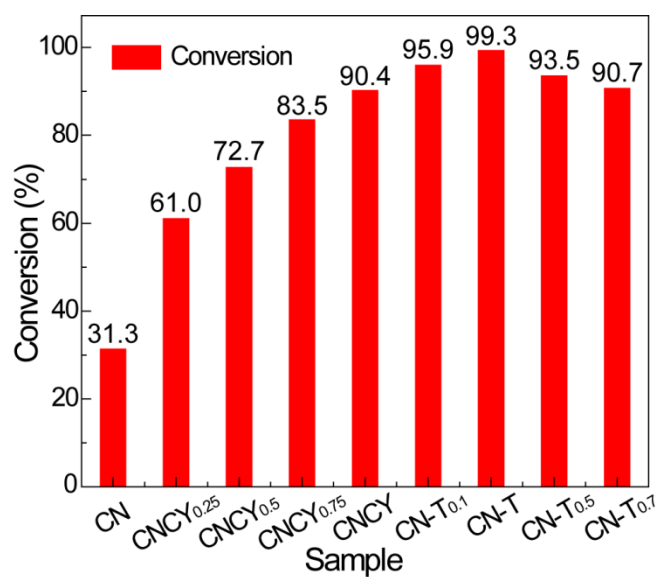


Figure S1. Styrene conversion rate as the function of cyano group content in carbon nitride.

Reaction condition: 0.04 mmol of the styrene, 2 mL of the acetonitrile, 10 μ L of the isobutyraldehyde, 15 mg of the catalyst, 1 atm Air, 400 mW/cm² irradiation, white LED light, 60 °C, 2 h.

The isobutyraldehyde was used as the reduction reagent, the selectivity for styrene oxide by using CN and CN-T is 45% and 87%, respectively. Thus, the yield of styrene oxide by using CN and CN-T is 14.1% and 86.4%, respectively.

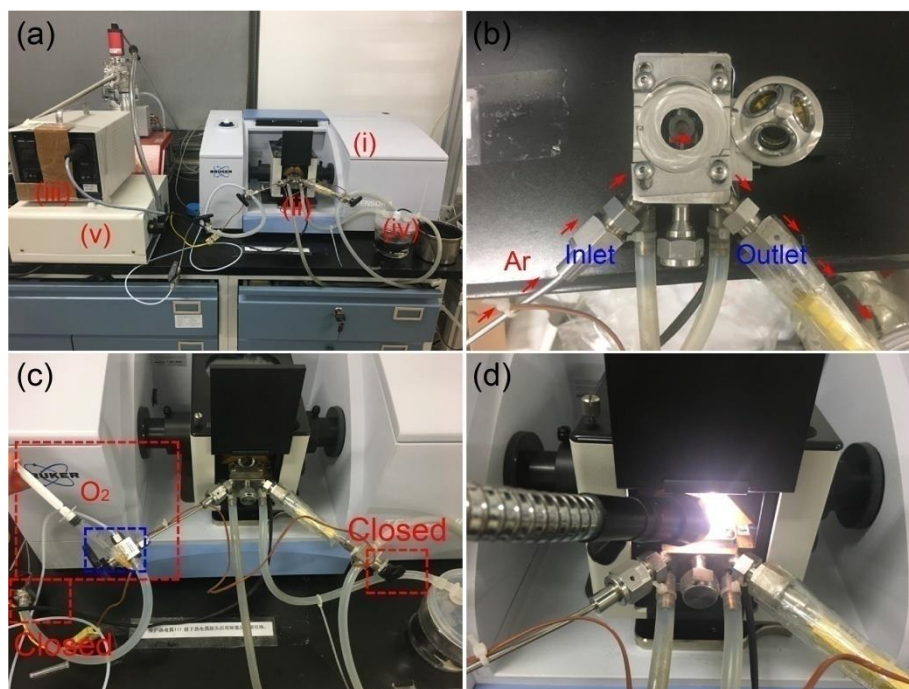


Figure S2. Photographs of (a) *in-situ* FT-IR setup. (b) HVC accessory enclosed with a three-window dome. (c) Oxygen injection methods. (d) Light illumination.

In [Figure S2](#), the digital coding represents (i) Bruker Tensor II FTIR spectrometer, (ii) HVC accessory, (iii) HARRICK ATC-024-4 temperature controller, (iv) cooling water circulating system and (v) Xenon lamp. Before the oxygen injection, the two three-way valves (red box) in [Figure S2c](#) were closed. The oxygen (5 mL) was injected by using 2.5 mL needle tube, after that the three-way valve in the blue box was closed until the end of the test.

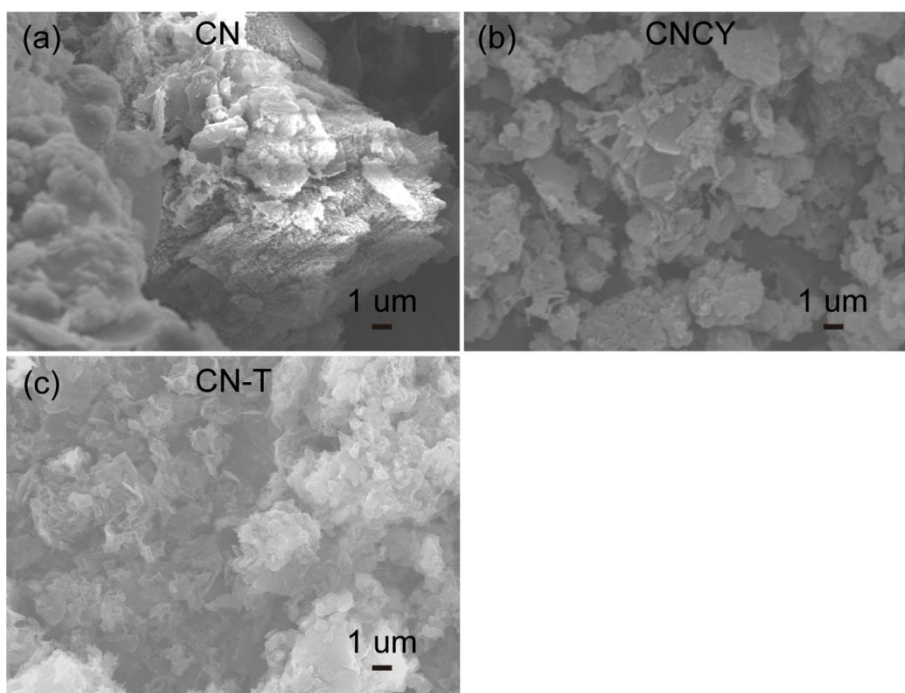


Figure S3. The SEM spectra of sample (a) CN, (b) CNCY and (c) CN-T.

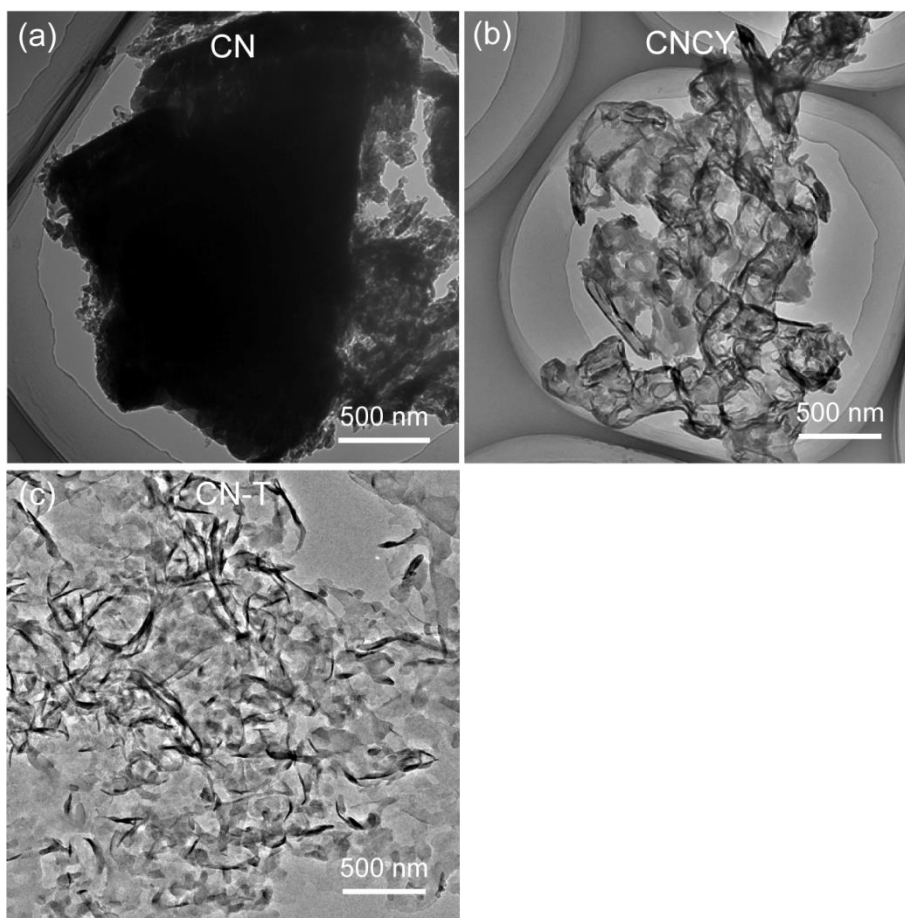


Figure S4. The TEM spectra of sample (a) CN, (b) CNCY and (c) CN-T.

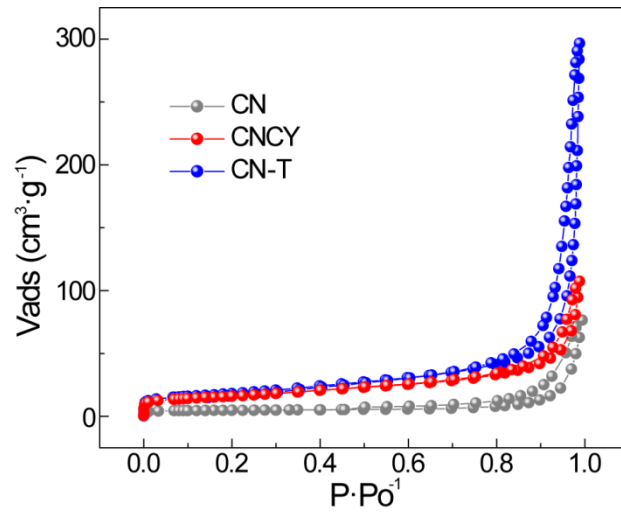


Figure S5. Adsorption isotherms spectra of CN, CNCY and CN-T.

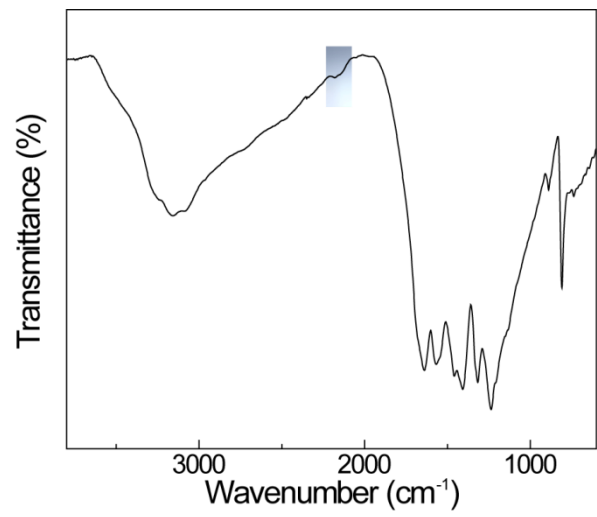


Figure S6. The FT-IR spectra of CN_{th}.

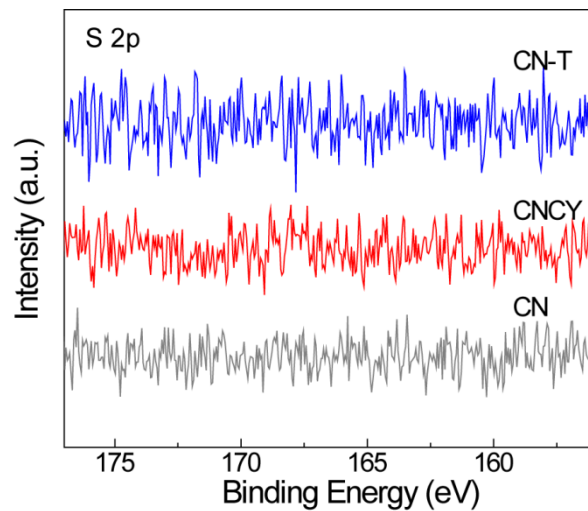


Figure S7. S 2p spectra of CN, CNCY and CN-T.

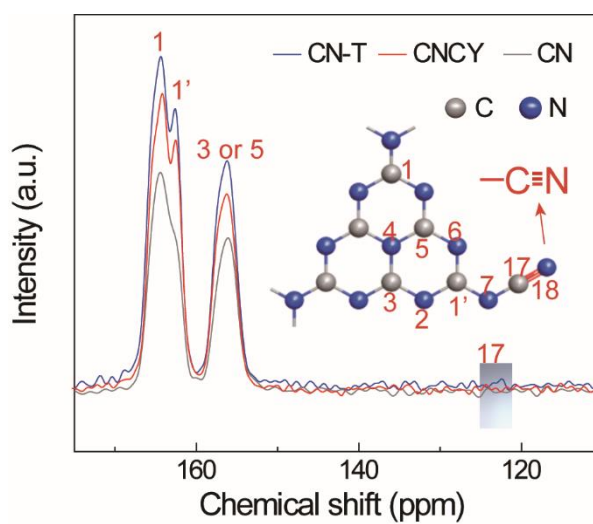


Figure S8. Solid-state ^{13}C MAS NMR spectra of CN, CNCY and CN-T.

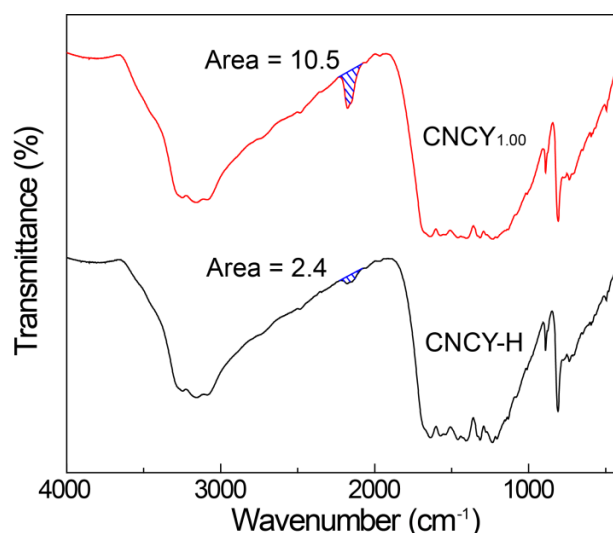


Figure S9. The FT-IR spectra of CNCY and CNCY-H.

As shown in [Figure S9](#), after sample CNCY was refluxed in 3M sulphuric acid for 2 h, the cyano area which calculated by using the OMNIC software is decreased from 10.5 to 2.4. That indicates about 77.1% of the cyano group had been hydrolyzed to carboxylic acid. The titration results of carboxyl group in CNCY_{1.00}-H is 0.40 mmol/g ([Table S5](#), entry 2), thus the total cyano content in CNCY_{1.00} is about 0.52 mmol/g ($0.4 / 0.771 = 0.52$) and the mass percent is about 1.5 wt% [$(0.52 \text{ mmol/g} \times 1 \text{ g} \times 26 \text{ g/mol}) / 1 \text{ g} \times 100 \text{ wt\%} = 1.5 \text{ wt\%}$]. The total cyano content in CN-T is about 0.62 mmol/g, then the mass percent is about 1.8 wt% [$(0.62 \text{ mmol/g} \times 1 \text{ g} \times 26 \text{ g/mol}) / 1 \text{ g} \times 100 \text{ wt\%} = 1.8 \text{ wt\%}$]. The treatment and cyano group conversion methods of other samples in entries 3-10 were same to CNCY and CN-T. The detailed cyano group content of each sample was summarized in [Table S5](#).

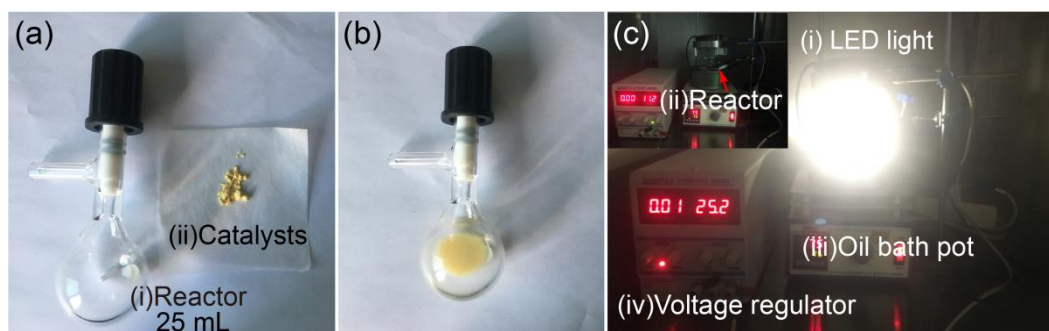


Figure S10. Images of the experimental setups for (a) reactor (b) with reactant and catalyst loaded and (c) photocatalytic oxidation reactions.

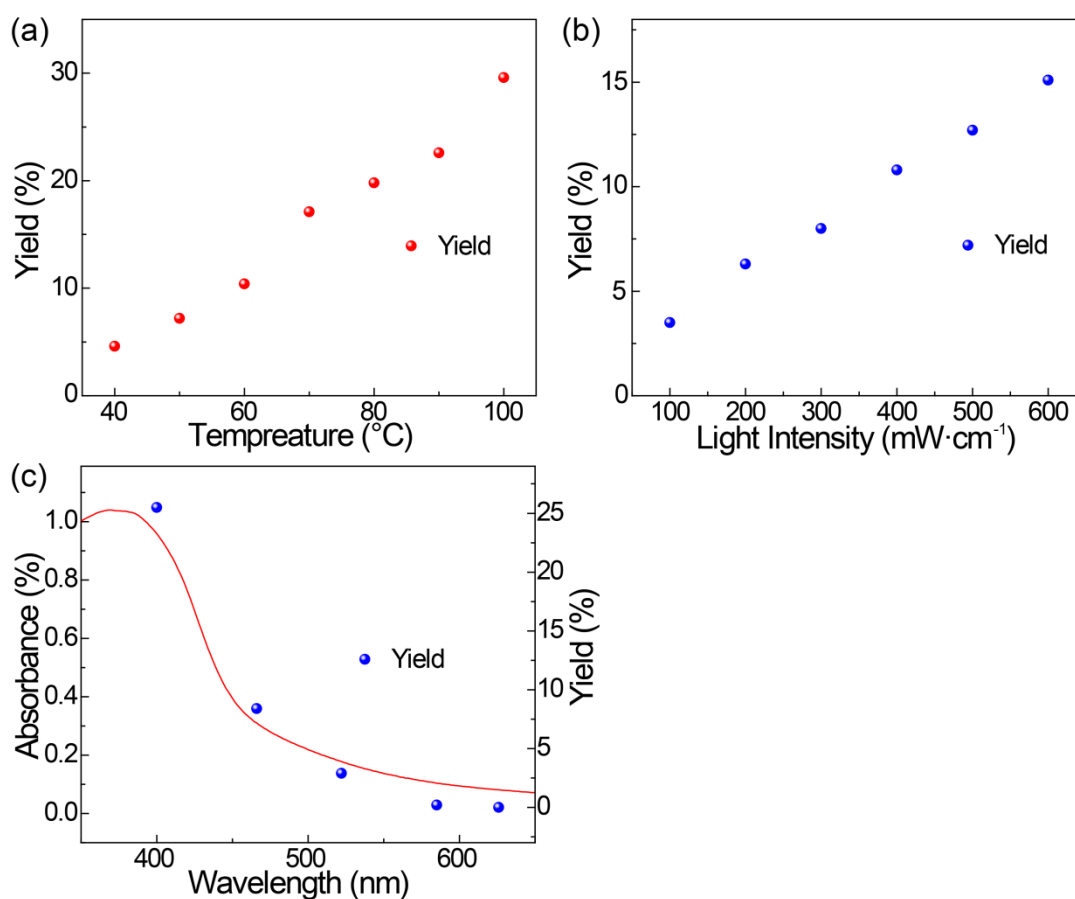


Figure S11. Influence of (a) temperature (b) light intensity and (c) wavelength (purple 400 nm, blue 459 nm, green 525 nm, yellow 580 nm, red 625 nm) on the epoxidation of styrene.

Reaction condition: 0.04 mmol of styrene, 2 mL of acetonitrile, 10 mg of the catalyst, 1 atm Air, white LED light, 4 h. (a) 400 mW/cm² irradiation, (b) 60 °C (c) 400 mW/cm² irradiation, 60 °C.

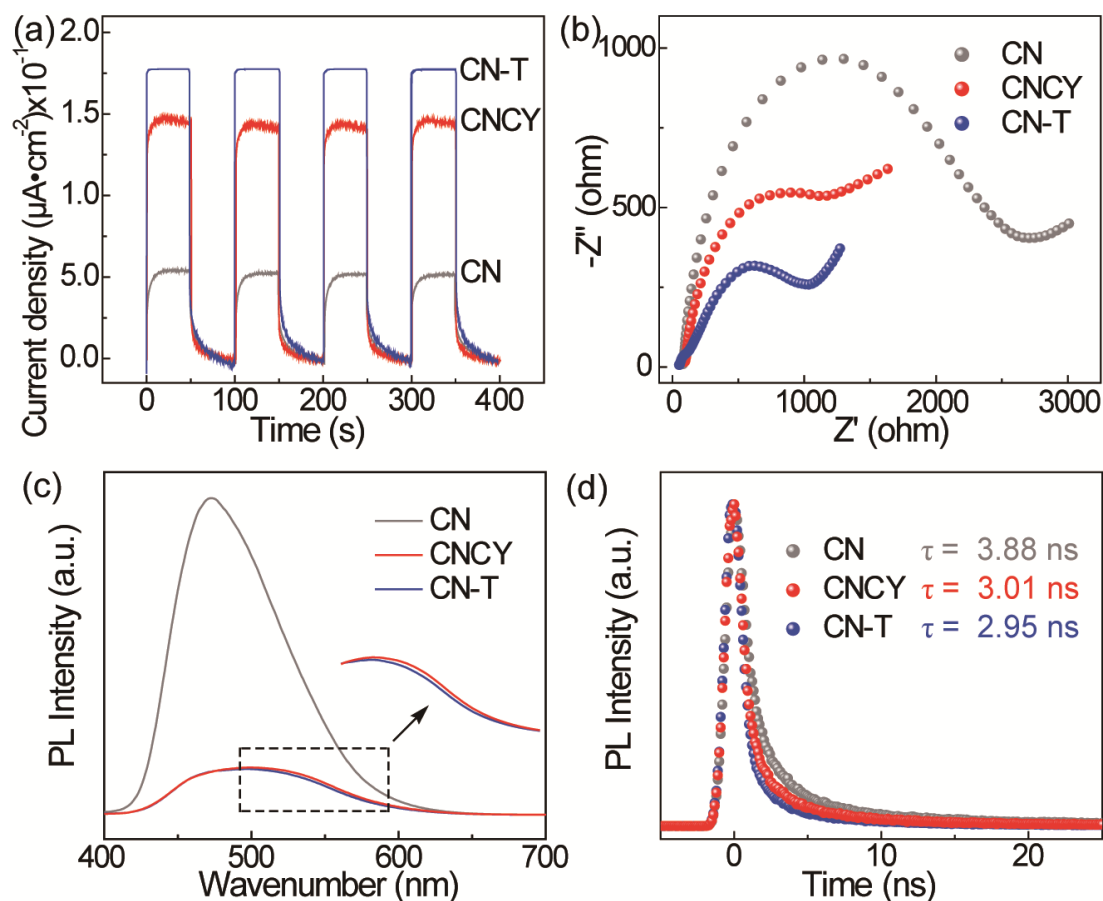


Figure S12. Optical, electronic properties and catalytic performance of varied carbon nitride catalysts. (a) Photocurrent response. (b) EIS Nyquist plots of CN, CNCY and CN-T. (c) Steady-state and (d) time-resolved photoluminescence decay spectra of CN, CNCY and CN-T at $\lambda_{\text{ex}} = 365$ nm.

The generation and separation efficiency of photogenerated carriers were measured by three classic methods: transient photocurrent, electrochemical impedance spectroscopy and photoluminescence.¹² The transient photocurrent of the samples was prompted by the on/off of intermittent visible-light irradiation ($\lambda > 420$ nm) in 0.2 M Na_2SO_4 aqueous solution. An obvious increase of photocurrent density was observed from CN to CNCY and CN-T (Figure S12a). The electrochemical impedance spectroscopy (EIS) in the dark was carried out. It can be seen that the arc radius decreases in the order of CN > CNCY > CN-T, indicating less resistance of charge

across the cyano modified sample film electrode interface (Figure S12b).¹³ The steady-state photoluminescence (PL) and the time-resolved PL spectra were monitored under the excitation wavelength of 365 nm. For CN, the strong PL emission at 470 nm shows high charge carriers recombination efficiency. After cyano group modification, the intensity of this emission peak is weakened (Figure S12c). Time-resolved PL yield the mean radiative lifetimes of 3.88, 3.01 and 2.95 ns for CN, CNCY and CN-T, respectively (Figure S12d). The decreased singlet exciton lifetime clearly suggests enhanced singlet exciton dissociation and more effective separation of photogenerated electron-hole pairs in CN-T,¹⁴ which is consistent with the result of photocurrent and EIS result. These results all indicate that the cyano group modification could improve the carrier generation and separation efficiency.¹⁵

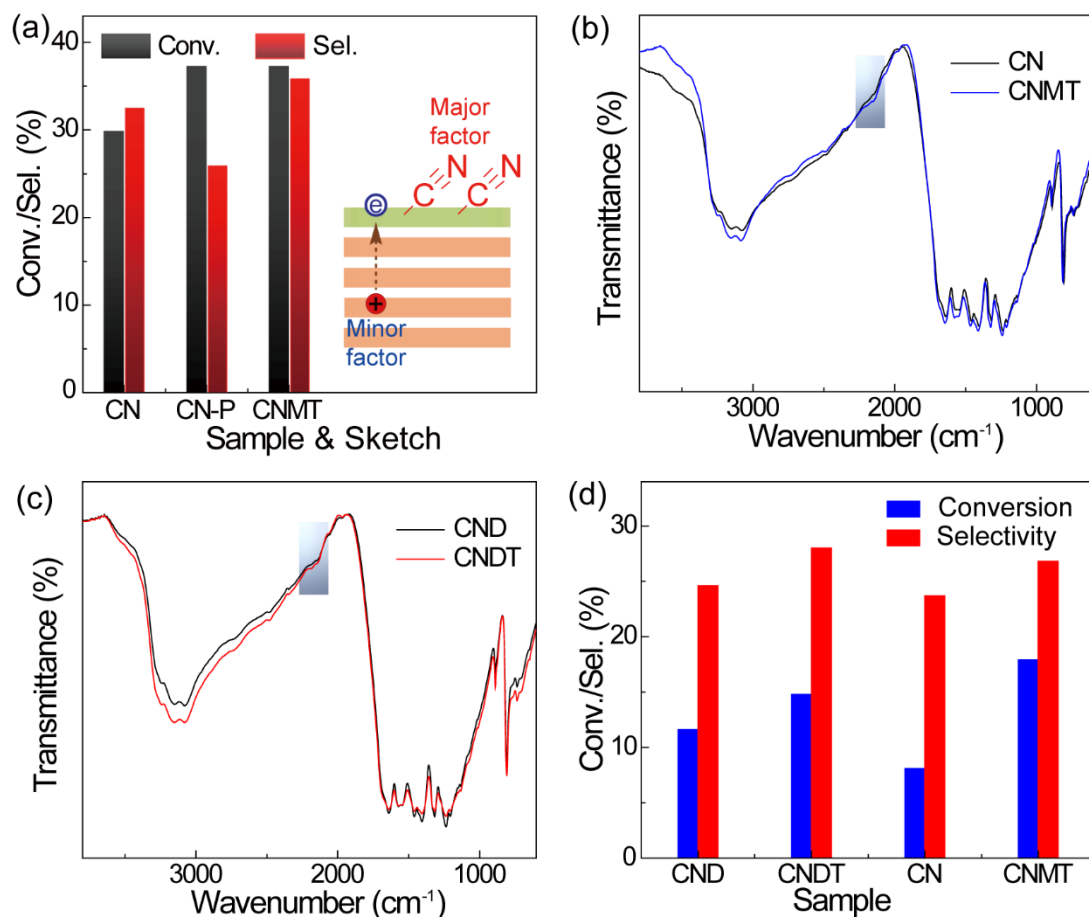


Figure S13. Catalytic performance comparison between CN, CN-P and CNMT for epoxidation of styrene. The inset diagram in Figure S13a is the sketch exhibited the major and minor factor which affect the performance of the catalyst. FT-IR spectra of (b) CN, CNMT and (c) CND, CNDT. (d) Catalytic performance comparison between CN, CNMT, CND and CNDT for epoxidation of styrene.

Reaction conditions: 0.04 mmol of styrene, 2 mL of acetonitrile, 15 mg of catalyst, 1 atm air, 400 mW/cm², white LED light irradiation, 60 °C, 4 h. Selectivity = Selectivity for styrene oxide.

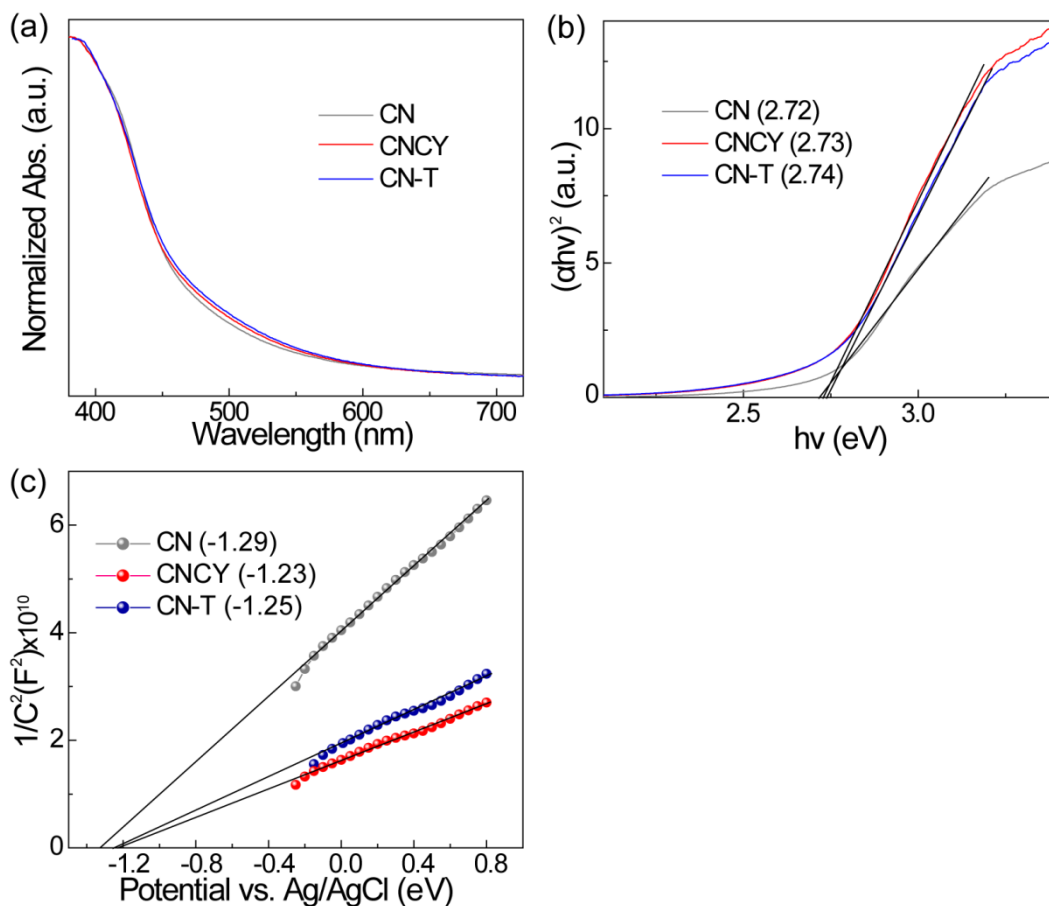


Figure S14. (a) UV-Vis patterns (b) band gap energy and (c) Mott-Schottky plots.

The band gap obtained from UV-Vis curves of CN, CNCY and CN-T were 2.72, 2.73 and 2.74 eV, respectively (Figure S14a and b). That indicates cyano group modifying caused a slightly enlarged band gap, which attributes to the quantum effect caused by formation thin layer structure.¹⁶ However, this does not affect the utilization the energy of light. On account of sample CNCY and CN-T showed a tail absorption (Urbach tail) in the visible-light region (Figure S14a), which indicates that a midgap state is created by the cyano introduction.¹² Thus, the CNCY_x samples can absorb more visible light, which will promote the solar light utilization efficiency. The Mott-Schottky curves showed in Figure S14c indicate a typical *n*-type plot for all samples. According to these plots, the flat band potentials of CN, CNCY, and CN-T were determined to be

at -1.29, -1.23 and -1.25 V vs. Ag/AgCl at pH = 6.6, which correspond to -0.76 V, -0.64 V and -0.66 V vs. SHE at pH = 0, respectively (according to eq. s5 and eq. s6)

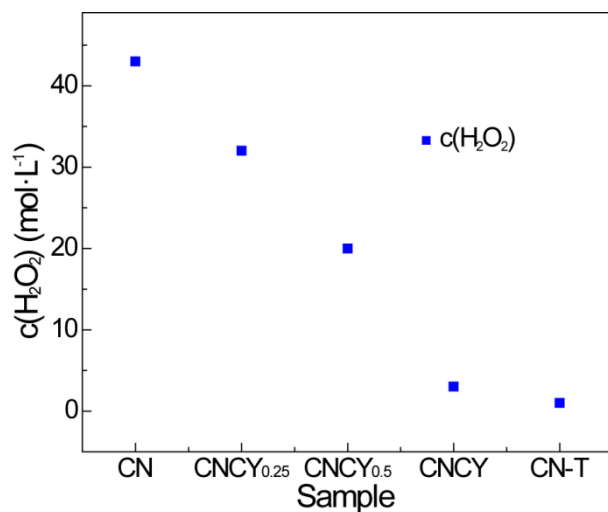


Figure S15. (a) The yield of H₂O₂ as the function of various catalysts.

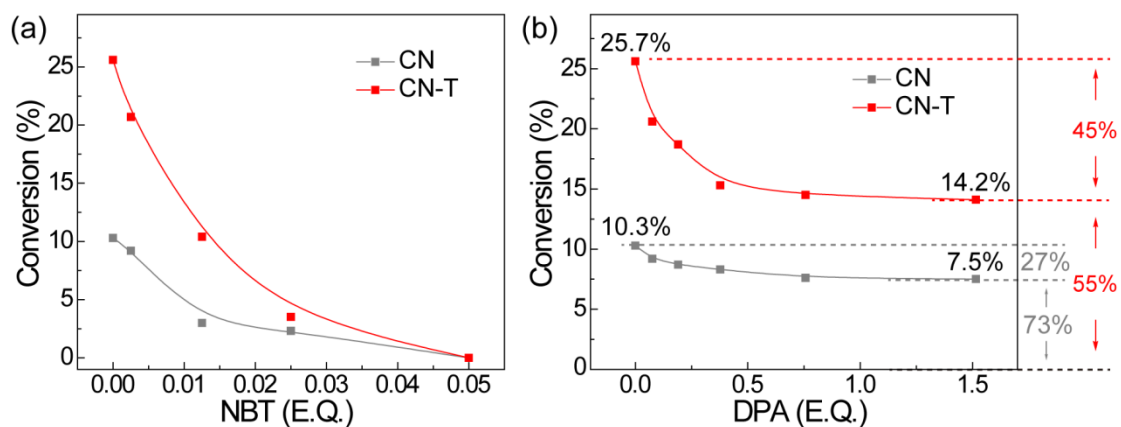


Figure S16. (a) Conversion and selectivity of styrene oxide as the function of nitroblue tetrazolium amount (NBT) and (b) 9,10-Diphenylanthracene (DPA) amount.

Reaction conditions: 0.04 mmol of the styrene, 2 mL of the acetonitrile, 10 mg of the catalyst, 1 atm Air, 400 mW/cm² irradiation, white LED light, 60 °C, 4 h.

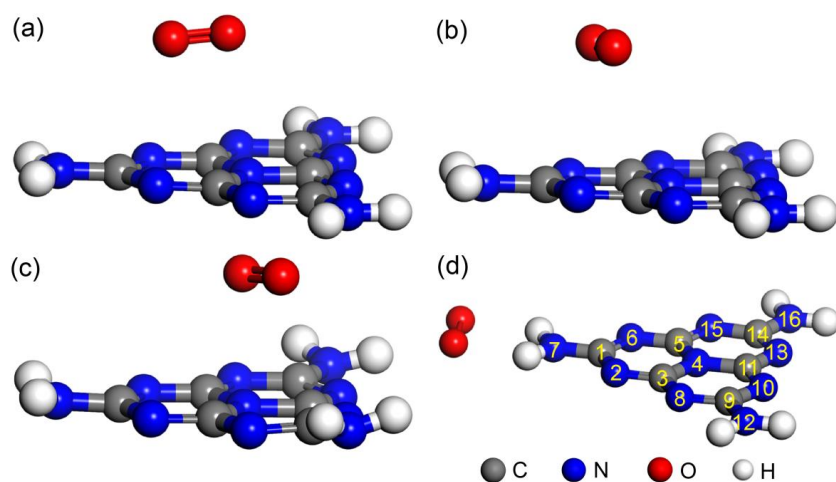


Figure S17. The optimized dioxygen adsorption mode on CN. The single-state O₂ initially located above the (a)N4-C1, (b) N6-C3, (c) N4-C11, and (d) N7-C1.

After the interaction of single-state O₂ with CN, the optimized configurations in [Figure S17a](#) is the most stable compared to the other adsorption configurations, in which the single-state O₂ is located above the N4-C1 site, the adsorption energy was summarized in [Table S7](#).

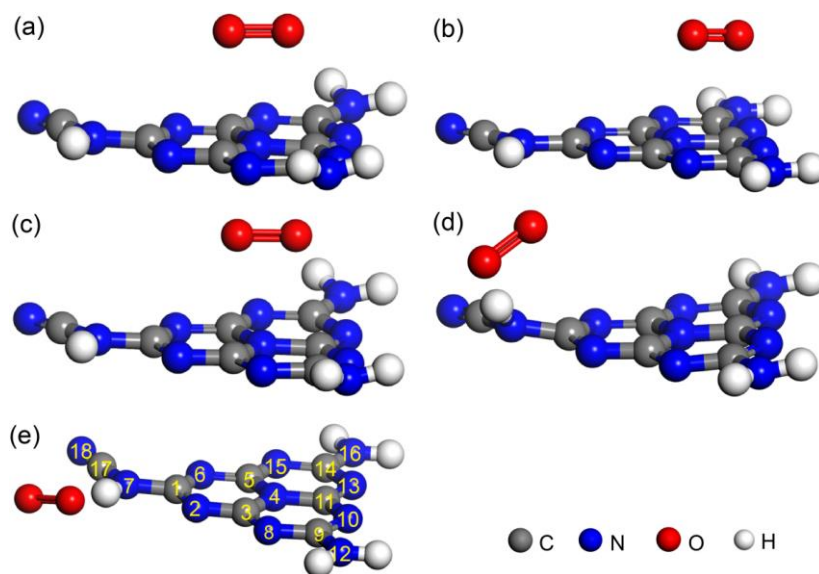


Figure S18. Other five types of the optimized dioxygen adsorption mode on cyano modified carbon nitride. The single-state O₂ initially located above the (a) N4-C1, (b) C3-N10, (c) N4-C11, (d) C17-N18 and (e) N7-H.

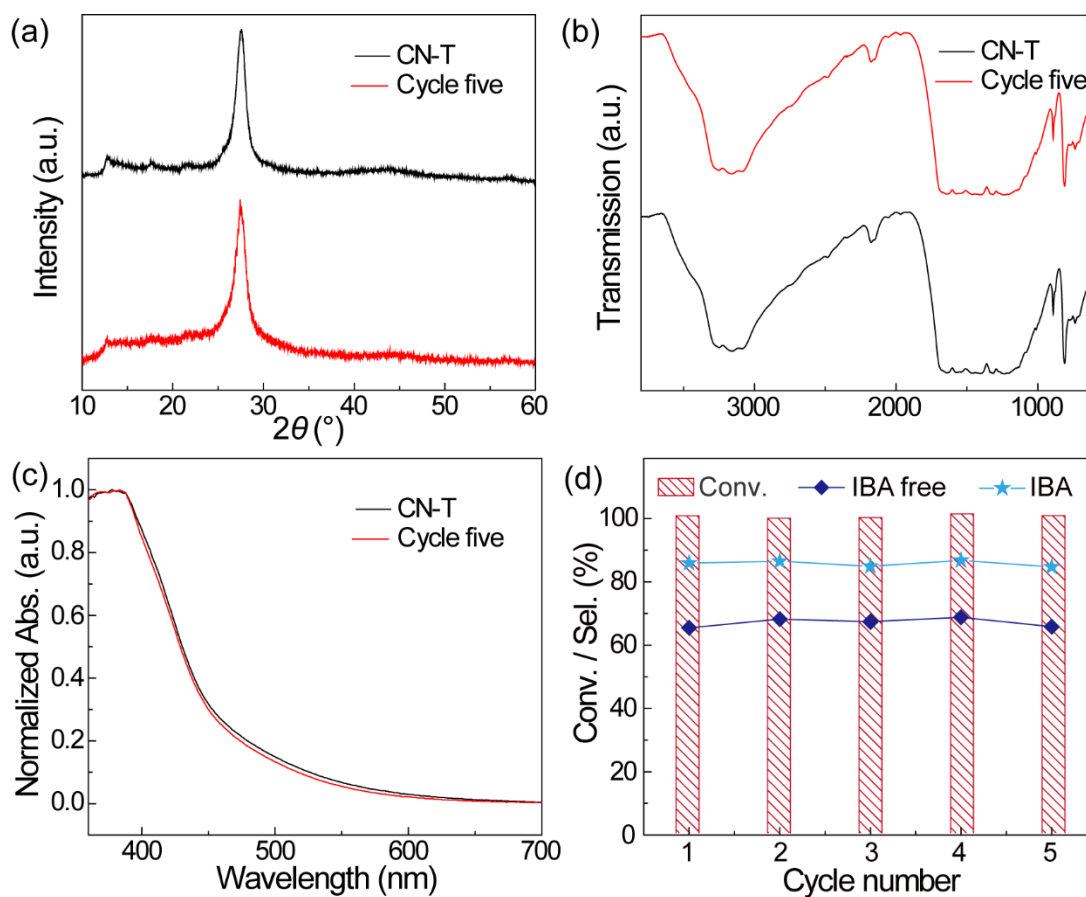


Figure S19. (a) XRD (b) FT-IR and (c) UV-Vis patterns of sample CN-T after being recycled five times. (d) Cycling performance of CN-T. Diamond: the epoxy products selectivity in the absence of isobutyraldehyde (IBA) as reducing agent. Star: the epoxy products selectivity in the presence of IBA.

Reaction conditions: 0.04 mmol of styrene, 2 mL of acetonitrile, 10 mg of catalyst, 1 atm air, white LED illumination (400 mW/cm^2), 60°C , 24 h for isobutyraldehyde free and 2 h for isobutyraldehyde added system.

Table S1. Summary of the yield of styrene oxide in 15 literatures.

Entry	Samples	Conv. (%)	Sel. _{epoxide} (%)	Yield _{epoxide} (%)	Ref
1	Fe ²⁺ -NaY	46.2	62.2	28.7	17
2	Fe ₃ O ₄	38.0	56.5	21.5	17
3	Co ²⁺ -X	44.2	60.0	26.5	18
4	CoCl ₂	90.0	0	0	19
5	Co-Y-ZrO ₂	61.0	80.0	48.8	20
6	Ga-Co-HMS-X	99.9	67.5	67.4	21
7	NHPI/Fe(BTC)	7.0	14.0	1.0	22
8	AuNC@N-C	96.8	40.4	39.1	23
9	La-MCM-48	54.5	98.8	53.8	24
10	N-OLC	88.4	46.0	40.7	25
11	OMCA-10	75.8	56.6	42.9	26
12	BaO/Ga ₂ O ₃	49.3	58.0	28.6	27
13	VS-1(1)	70.0	44.0	30.8	28
14	Au ₂₅ (SR) ₁₈	36.6	32.0	11.7	29
15	Ti(OiPr) ₄ /ligand	73.0	71.0	51.8	30
16	P450 enzymes	96.0	50.0	48.0	31

Table S2. Physicochemical properties of CN, CNCY and CN-T.

Sample	Pore volume (cm ³ /g)	S _{BET} (m ² /g)
CN	0.12	14.2
CNCY	0.37	61.3
CN-T	0.45	65.6

Table S3. Distribution of element species obtained from the deconvolution of the N1s peaks by XPS.

Sample	Area / Proportion (%)		
	C-N=C	N-(C) ₃	C-N-H
CN	80626.8 / 74.0%	24289.3 / 22.3%	4096.2 / 3.8%
CNCY	93936.4 / 74.2%	28330.6 / 22.4%	4303.8 / 3.4%
CN-T	76891.8 / 74.2%	23710.3 / 22.9%	3060.2 / 3.0%

The proportion of C-N-H component was calculated by dividing the peak area of C-N-H by the total area.

Table S4. Distribution of element species obtained from the deconvolution of the C1s peaks by XPS.

Sample	Area			Area _(C-NH_x & C≡N)
	C-C	N-C=N	C-NH _x & C≡N	/ Area _(N-C=N)
CN	6259.6	45623.4	1406.2	0.03
CNCY	1165.5	47448.7	1423.5	0.03
CN-T	12187.6	43421.9	1302.7	0.03

The proportion of C-H_x & C≡N component was calculated by dividing the peak area of C-H_x & C≡N by the area of N-C=N.

Table S5. The content variation of cyano and carboxyl groups on the cyano modified samples.

Entry	Sample	Cyano group area	Conv._{area} (%)	Carboxyl (mmol/g)	Cyano group Estimated value (mmol/g)
1	CNCY	10.5	0	0	0
2	CNCY-H	2.4	77.1	0.40	0.52
3	CNCY _{0.25}	2.3	0	0	0
4	CNCY _{0.25} -H	0.56	75.6	0.08	0.11
5	CNCY _{0.40}	3.8	0	0	0
6	CNCY _{0.40} -H	0.72	81.1	0.15	0.19
7	CNCY _{0.50}	5.0	0	0	0
8	CNCY _{0.50} -H	1.07	78.6	0.20	0.25
9	CNCY _{0.75}	7.8	0	0	0
10	CNCY _{0.75} -H	1.61	79.3	0.31	0.39
11	CN-T	12.6	78.6	0.49	0.62
12	CN-T-H	2.7	0	0	0

Table S6. The catalytic and photoelectric performance of CN and CN-P.

Entry	Sample	Conv. (%)	Sel. _{styrene} oxide (%)	Photocurrent	Electrochemic	Fluorescence
				density ($\mu\text{A}/\text{cm}^2$)	al impedance (Ω)	lifetime (ns)
1	CN	31.9	33.6	0.051	4800	3.88
2	CN-P	37.5	25.4	0.062	3100	3.56

Reaction condition: 0.04 mmol of styrene, 2 mL of acetonitrile, 10 mg of the catalyst, 1 atm Air, 60 °C, white LED light, 400 mW/cm² irradiation, 12 h.

The CN-P sample was prepared by heating melamine (10 g) and ammonium phosphate (0.25 g) mixture in a muffle furnace at 550 °C for 4 h.

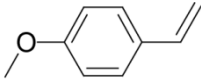
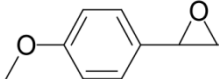
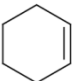
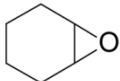
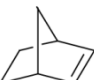

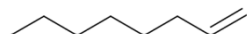
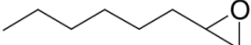
Table S7. The adsorption energy related Figure S16.

Entry	Initial site	Total energy (Ha)	Relative energy
			(kJ/mol)
1	N4-C1	-929.5073504	-39.1
2	N6-C3	-929.5009105	-22.2
3	N4-C11	-929.494547	-5.5
4	N7-C1	-929.4924522	0.0

Table S8. The adsorption energy related Figure S17.

Entry	Initial site	Total energy (Ha)	Relative energy (kJ/mol)
1	N7-C17	-1021.647935	-39.3
2	N7-N18	-1021.647874	-39.1
3	N4-C1	-1021.643873	-28.6
4	C3-N10	-1021.643673	-28.1
5	N4-C11	-1021.643933	-28.8
6	C17-N18	-1021.639660	-17.5
7	N7-H	-1021.632977	0.0

Table S9. Scope of the CN-T catalyzed epoxidation reaction of alkenes.

Entry	Substrates	Products	Conversion (%)	Selectivity (%)
1			99.6	65.8
2			99.6	54.5
3			99.9	99.9
4			13	60.1

Reaction conditions: 0.04 mmol of the alkenes, 2 mL of the acetonitrile, 10 mg of the catalyst, 1

atm Air, 400 mW/cm² irradiation, white LED light, 60 °C, 24 h.

Supplemental References

1. Lau, V.W.H., Moudrakovski, I., Botari, T., et al. Rational Design of Carbon Nitride Photocatalysts by Identification of Cyanamide Defects as Catalytically Relevant Sites. *Nat. Commun.* **7**, 12165-12174 (2016). 10.1038/ncomms12165 <https://www.nature.com/articles/ncomms12165#supplementary-information>
2. Niu, P., Qiao, M., Li, Y., et al. Distinctive Defects Engineering in Graphitic Carbon Nitride for Greatly Extended Visible Light Photocatalytic Hydrogen Evolution. *Nano Energy* **44**, 73-81 (2018). <https://doi.org/10.1016/j.nanoen.2017.11.059>
3. Yuan, B., Chu, Z., Li, G., et al. Water-Soluble Ribbon-Like Graphitic Carbon Nitride (*g*-C₃N₄): Green Synthesis, Self-Assembly and Unique Optical Properties. *J. Mater. Chem. C* **2**, 8212-8215 (2014). 10.1039/C4TC01421A
4. Yu, H., Shi, R., Zhao, Y., et al. Alkali-Assisted Synthesis of Nitrogen Deficient Graphitic Carbon Nitride with Tunable Band Structures for Efficient Visible-Light-Driven Hydrogen Evolution. *Adv. Mater.* **29**, 1605148-1605156 (2017). 10.1002/adma.201605148
5. Liu, G., Zhao, G., Zhou, W., et al. In Situ Bond Modulation of Graphitic Carbon Nitride to Construct p-n Homojunctions for Enhanced Photocatalytic Hydrogen Production. *Adv. Funct. Mater.* **26**, 6822-6829 (2016). 10.1002/adfm.201602779
6. Delley, B. An All-Electron Numerical-Method for Solving the Local Density Functional for Polyatomic-Molecules. *J Chem. Phys.* **92**, 508-517 (1990). 10.1063/1.458452
7. Delley, B. From Molecules to Solids with the DMol³ Approach. *J Chem. Phys.* **113**, 7756-7764 (2000). 10.1063/1.1316015
8. Tian, D., Zhang, H. and Zhao, J. Structure and Structural Evolution of Ag_n (n=3–22) Clusters using a Genetic Algorithm and Density Functional Theory Method. *Solid State Commun.* **144**, 174-179 (2007). <https://doi.org/10.1016/j.ssc.2007.05.020>
9. Perdew, J.P., Burke, K. and Ernzerhof, M. Generalized Gradient Approximation Made Simple. *Phys. Rev. Lett.* **77**, 3865-3868 (1996). 10.1103/PhysRevLett.77.3865
10. Hohenberg, P. and Kohn, W. Inhomogeneous Electron Gas. *Phys. Rev.* **136**, B864-B871 (1964). 10.1103/PhysRev.136.B864
11. Inada, Y. and Orita, H. Efficiency of Numerical Basis Sets for Predicting the Binding Energies of Hydrogen Bonded Complexes: Evidence of Small Basis Set Superposition Error Compared to Gaussian Basis Sets. *J. Comput. Chem.* **29**, 225-232 (2008). 10.1002/jcc.20782
12. Tan, H., Gu, X., Kong, P., et al. Cyano Group Modified Carbon Nitride with Enhanced Photoactivity for Selective Oxidation of Benzylamine. *Appl. Catal. B. Environ.* **242**, 67-75 (2019). <https://doi.org/10.1016/j.apcatb.2018.09.084>
13. Wang, J., Yang, Z., Yao, W., et al. Defects Modified in the Exfoliation of *g*-C₃N₄ Nanosheets Via a Self-Assembly Process for Improved Hydrogen Evolution Performance. *Appl. Catal. B. Environ.* **238**, 629-637 (2018). <https://doi.org/10.1016/j.apcatb.2018.07.017>
14. Ou, H., Chen, X., Lin, L., et al. Biomimetic Donor-Acceptor Motifs in Conjugated Polymers for Promoting Exciton Splitting and Charge Separation. *Angew. Chem. Int. Ed.* **57**, 8729-8733 (2018). 10.1002/anie.201803863

15. Li, Y., Ouyang, S., Xu, H., et al. Constructing Solid–Gas-Interfacial Fenton Reaction over Alkalinized-C₃N₄ Photocatalyst to Achieve Apparent Quantum Yield of 49% at 420 nm. *J. Am. Chem. Soc.* **138**, 13289-13297 (2016). 10.1021/jacs.6b07272
16. Xiao, Y., Tian, G., Li, W., et al. Molecule Self-Assembly Synthesis of Porous Few-Layer Carbon Nitride for Highly Efficient Photoredox Catalysis. *J. Am. Chem. Soc.* **141**, 2508-2515 (2019). 10.1021/jacs.8b12428
17. Liang, J., Zhang, Q., Wu, H., et al. Iron-Based Heterogeneous Catalysts for Epoxidation of Alkenes using Molecular Oxygen. *Catal. Commun.* **5**, 665-669 (2004). <https://doi.org/10.1016/j.catcom.2004.08.010>
18. Tang, Q., Wang, Y., Liang, J., et al. Co²⁺-Exchanged Faujasite Zeolites as Efficient Heterogeneous Catalysts for Epoxidation of Styrene with Molecular Oxygen. *Chem. Commun.*, 440-441 (2004). 10.1039/B314864E
19. Lin, Y.H., Williams, I.D. and Li, P. Selective Oxidation of Styrenes under Oxygen Catalyzed by Cobalt Chloride. *Appl Catal A-Gen* **150**, 221-229 (1997). [https://doi.org/10.1016/S0926-860X\(96\)00187-1](https://doi.org/10.1016/S0926-860X(96)00187-1)
20. Tyagi, B., Shaik, B. and Bajaj, H.C. Epoxidation of Styrene with Molecular O₂ over Sulfated Y–ZrO₂ Based Solid Catalysts. *Appl Catal A-Gen* **383**, 161-168 (2010). <https://doi.org/10.1016/j.apcata.2010.05.038>
21. Rahman, S., Santra, C., Kumar, R., et al. Highly Active Ga Promoted Co-HMS-X Catalyst Towards Styrene Epoxidation Reaction using Molecular O₂. *Appl. Catal. A: Gen.* **482**, 61-68 (2014). <https://doi.org/10.1016/j.apcata.2014.05.024>
22. Dhakshinamoorthy, A., Alvaro, M. and Garcia, H. Aerobic Oxidation of Styrenes Catalyzed by an Iron Metal Organic Framework. *ACS Catal.* **1**, 836-840 (2011). 10.1021/cs200128t
23. Liu, B., Wang, P., Lopes, A., et al. Au–Carbon Electronic Interaction Mediated Selective Oxidation of Styrene. *ACS Catal.* **7**, 3483-3488 (2017). 10.1021/acscatal.7b01048
24. Zhan, W., Guo, Y., Wang, Y., et al. Study of Higher Selectivity to Styrene Oxide in the Epoxidation of Styrene with Hydrogen Peroxide over La-Doped MCM-48 Catalyst. *J. Phys. Chem. C* **113**, 7181-7185 (2009). 10.1021/jp8101095
25. Lin, Y., Pan, X., Qi, W., et al. Nitrogen-Doped Onion-Like Carbon: A Novel and Efficient Metal-Free Catalyst for Epoxidation Reaction. *J. Mater. Chem. A* **2**, 12475-12483 (2014). 10.1039/C4TA01611D
26. Pan, D., Xu, Q., Dong, Z., et al. Facile Synthesis of Highly Ordered Mesoporous Cobalt–Alumina Catalysts and Their Application in Liquid Phase Selective Oxidation of Styrene. *RSC Adv.* **5**, 98377-98390 (2015). 10.1039/C5RA20531J
27. Choudhary, V.R., Jha, R. and Jana, P. Epoxidation of Styrene by TBHP to Styrene Oxide using Barium Oxide as a Highly Active/Selective and Reusable Solid Catalyst. *Green Chem.* **8**, 689-690 (2006). 10.1039/B604937K
28. Singh, B. and Sinha, A.K. Synthesis of Hierarchical Mesoporous Vanadium Silicate-1 Zeolite Catalysts for Styrene Epoxidation with Organic Hydroperoxide. *J. Mater. Chem. A* **2**, 1930-1939 (2014). 10.1039/C3TA13451B
29. Zhu, Y., Qian, H., Zhu, M. and Jin, R. Thiolate-Protected Au Nanoclusters as Catalysts for Selective Oxidation and Hydrogenation Processes. *Adv. Mater.* **22**, 1915-1920 (2010). 10.1002/adma.200903934

30. Matsumoto, K., Oguma, T. and Katsuki, T. Highly Enantioselective Epoxidation of Styrenes Catalyzed by Proline-Derived C1-Symmetric Titanium(Salan) Complexes. *Angew. Chem. Int. Ed.* **48**, 7432-7435 (2009). 10.1002/anie.200903567
31. Wang, L., Wei, S., Pan, X., et al. Enhanced Turnover for the P450 119 Peroxygenase-Catalyzed Asymmetric Epoxidation of Styrenes by Random Mutagenesis. *Chem.Eur.J.* **24**, 2741-2749 (2018). 10.1002/chem.201705460